An Investigation of Sting Interference Effects on an Oscillating Cone in Transonic Flow

Frederic B. Cyran
ARO, Inc.

August 1981

Final Report for Period September 26 — October 3, 1979

**ARNOLD ENGINEERING DEVELOPMENT CENTER
ARNOLD AIR FORCE STATION, TENNESSEE
AIR FORCE SYSTEMS COMMAND
UNITED STATES AIR FORCE**

This report has been reviewed by the Office of Public Affairs (PA) and is releasable to the National Technical Information Service (NTIS). At NTIS, it will be available to the general public, including foreign nations.

APPROVAL STATEMENT

This report has been reviewed and approved.

ALVIN R. OBAL, Captain, CF
Directorate of Technology
Deputy for Operations

Approved for publication:

FOR THE COMMANDER

MARION L. LASTER
Director of Technology
Deputy for Operations

REPORT DOCUMENTATION PAGE		READ INSTRUCTIONS BEFORE COMPLETING FORM
1 REPORT NUMBER AEDC-TR-80-66	2 GOVT ACCESSION NO.	3 RECIPIENT'S CATALOG NUMBER
4 TITLE (and Subtitle) AN INVESTIGATION OF STING INTERFERENCE EFFECTS ON AN OSCILLATING CONE IN TRANSONIC FLOW		5 TYPE OF REPORT & PERIOD COVERED Final Report, September 26 – October 3, 1979
		6. PERFORMING ORG. REPORT NUMBER
7 AUTHOR(s) Frederic B. Cyran, ARO, Inc., a Sverdrup Corporation Company		8 CONTRACT OR GRANT NUMBER(s)
9 PERFORMING ORGANIZATION NAME AND ADDRESS Arnold Engineering Development Center/DOT Air Force Systems Command Arnold Air Force Station, Tennessee 37389		10 PROGRAM ELEMENT, PROJECT, TASK AREA & WORK UNIT NUMBERS Program Element 65807F
11 CONTROLLING OFFICE NAME AND ADDRESS Arnold Engineering Development Center/DOS Air Force Systems Command Arnold Air Force Station, Tennessee 37389		12. REPORT DATE August 1981
		13. NUMBER OF PAGES 79
14 MONITORING AGENCY NAME & ADDRESS(if different from Controlling Office)		15. SECURITY CLASS. (of this report) UNCLASSIFIED
		15a DECLASSIFICATION/DOWNGRADING SCHEDULE N/A

16 DISTRIBUTION STATEMENT (of this Report)

Approved for public release; distribution unlimited.

17 DISTRIBUTION STATEMENT (of the abstract entered in Block 20, if different from Report)

18 SUPPLEMENTARY NOTES

Available in Defense Technical Information Center (DTIC).

19 KEY WORDS (Continue on reverse side if necessary and identify by block number)

wind tunnel tests	Reynolds number	critical sting length
sting mounts	forced oscillation technique	
conical bodies	base pressure	
stability	pitch damping	
boundary layer	angle of attack	

20 ABSTRACT (Continue on reverse side if necessary and identify by block number)

    Wind tunnel sting support interference effects on dynamic stability derivatives, static pitching moment and base pressure of a blunt, 7-deg cone were investigated at subsonic and transonic Mach numbers. The cone was tested with sting configurations having a variable effective sting length ranging from 1 to 3.3 model base diameters, at angles of attack ranging from 0 to 30 deg. A forced-oscillation system was utilized to obtain data at a frequency of oscillation of approximately 5.3 Hz, and at an amplitude of 1 deg.

DD FORM 1473 1 JAN 73   EDITION OF 1 NOV 65 IS OBSOLETE

20.   ABSTRACT, Concluded.

The Reynolds number, based on model base diameter, was nominally
1.8 million, which produced a turbulent boundary layer over the aft
portion of the model. The nature of the causes of these interfer-
ence effects is discussed and analyzed with respect to sting
length, type of measurement, and Mach number, with emphasis on
defining critical sting length and on predicting minimal interfer-
ence sting configurations for dynamic stability testing. The
results showed that the critical sting length depended on the type
of measurement used as the interference indicator, Mach number, and
angle of attack. A critical sting length of three model diameters
was determined to be suitable for all test conditions for the ratio
of sting diameter-to-model base diameter (0.22) investigated.

AFSC
Arnold AFS Tenn

PREFACE

The work reported herein was conducted by the Arnold
Engineering Development Center (AEDC), Air Force Systems Command
(AFSC). The results of the research were obtained by ARO, Inc.,
AEDC Group (a Sverdrup Corporation Company), operating contractor
for the AEDC, AFSC, Arnold Air Force Station, Tennessee, under
ARO Project Numbers P41C-A9 and V32F-09. The Air Force Project
Manager was Captain Alvin R. Obal (CF), AEDC/DOT. The data analysis
was completed on July 15, 1980, and the manuscript was submitted for
publication on October 27, 1980.

The material presented herein was submitted to the Univer-
sity of Tennessee, Knoxville, as partial fulfillment of the require-
ments of the degree of Master of Science. Mr. Cyran is currently
employed by Sverdrup Technology, Inc., AEDC Division.

TABLE OF CONTENTS

LIST OF FIGURES

CHAPTER I

INTRODUCTION

I. Background Information

Within the last few years, the demand for more
accurate wind tunnel data has led to increased emphasis on
the evaluation of support interference effects. If a wind
tunnel model is to be representative of the full-scale
vehicle, it must be mounted to a support system that will
not result in significant interference in the data. Since
it is difficult to separate interference from the actual
aerodynamics of the model, a support system must be chosen
carefully. A poorly chosen support may possibly cause the
aerodynamic measurements to be completely overshadowed by
interference effects. Thus, an understanding of the causes
of support interference is essential to the aerodynamicist
for predicting the aerodynamic characteristics of a vehicle
from wind tunnel data.

A wide variety of support systems may be used in a
wind tunnel, each having its own particular advantages and
disadvantages. Two of the most commonly used types of model
support systems are the strut support and the sting support.
The selection of the most appropriate support depends upon
the characteristics of the model to be tested and the kind
of data to be obtained. The present study will be limited

to a consideration of sting support interference, with emphasis on minimizing the interference relating to dynamic stability measurements within typical test constraints.

In an effort to obtain information on sting interference at transonic speed, an investigation of interference effects caused by sting configurations of various lengths was conducted. The objective of this investigation was to determine the effects of sting length on the measurements of pitch-damping derivatives, static pitching moment, and base pressure for a flat-base, slender cone. Although sting length effects are the primary focus of this investigation, effects caused by other geometric parameters of the sting (e.g., sting diameter effects, etc.) will also be discussed. Data from additional sources will also be used for comparisons.

Inherently, all physical support systems cause some interference by altering the flow field around the model. Since it is not possible to eliminate support interference completely, it can usually be minimized to such an extent as to be considered negligible. Some compromise is necessary because the support system must possess sufficient structural rigidity to support the model loads and also to provide a means for communicating the data from the model to the data recording system.

Although the presence of a sting alters the flow surrounding the model to some extent, it does not

necessarily result in significant interference on all aerodynamic parameters. Certain measurements are more sensitive to sting interference than others for a given model and test condition. This is governed by the proximity of the sting (or more specifically, the proximity of the flow field disturbances caused by the sting) to the location of the primary influences of a measurement. For example, consider the measurement of base pressure as compared to the measurement of pitching moment. Interference from a rear-mounted sting immersed in the base flow field will obviously affect the base pressure. However, pitching moment is primarily a function of the flow distribution over the entire surface of the model and is usually not influenced significantly by sting-induced disturbances in the base region.

Base pressure is generally accepted as being one of the most sensitive parameters to interference caused by a rear-mounted sting. Whitfield [1][1] reports that at supersonic speeds it can be used as a first indicator of sting interference, provided that interference-free base pressure data is known. A sting configuration having a minimal effect on base pressure could thus be confidently assumed to have an even smaller effect on other aerodynamic parameters. It is also easier in many cases to determine

------

[1]Numbers in brackets refer to similarly numbered references in the Bibliography.

if interference is present in the base pressure measurements than in other aerodynamic measurements.

However, any finite sting may affect base pressure by altering the size and location of the wake neck (Fig. 1), and for this reason base pressure is sometimes considered an overly sensitive parameter for estimating interference.

The subject of sting support interference on the measurement of a wide variety of aerodynamic parameters has been an area subject to considerable research within the last 30 years. A review of the references cited in Uselton and Cyran [2, 3], however, indicates the relative scarcity of interference data available at subsonic and transonic Mach numbers. Limited amounts of data at these Mach numbers were obtained by Lee and Summers [4], Love [5], Reese and Wehrend [6], and others [7, 8, 9]. These sources establish a broad spectrum of specific interference effects associated with limited configurations and test conditions, and primarily use base pressure as an interference indicator. Some confusion as to what constitutes a minimal interference sting configuration is also evident from these studies. Consequently, no general solution to the problem of sting interference is apparent in the available literature.
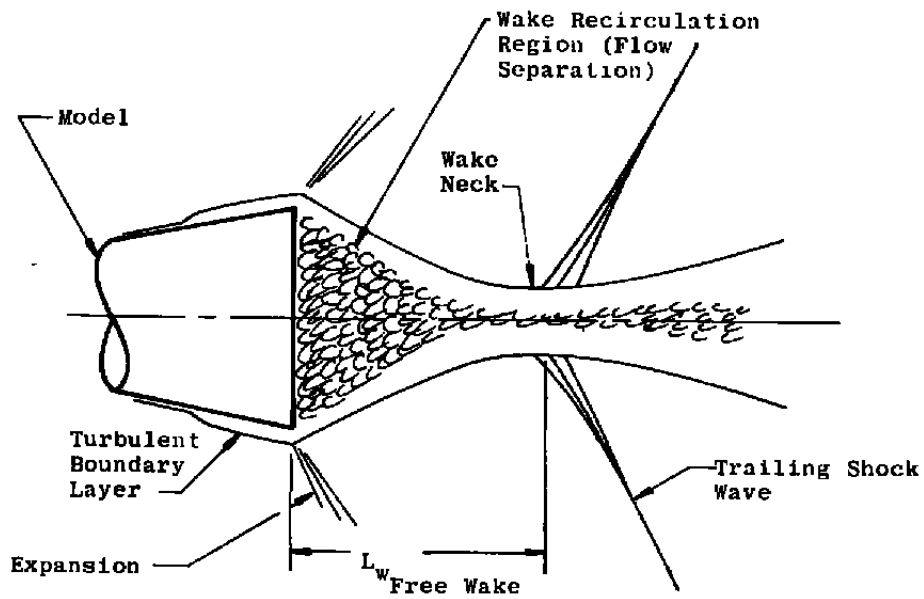
a. Free wake
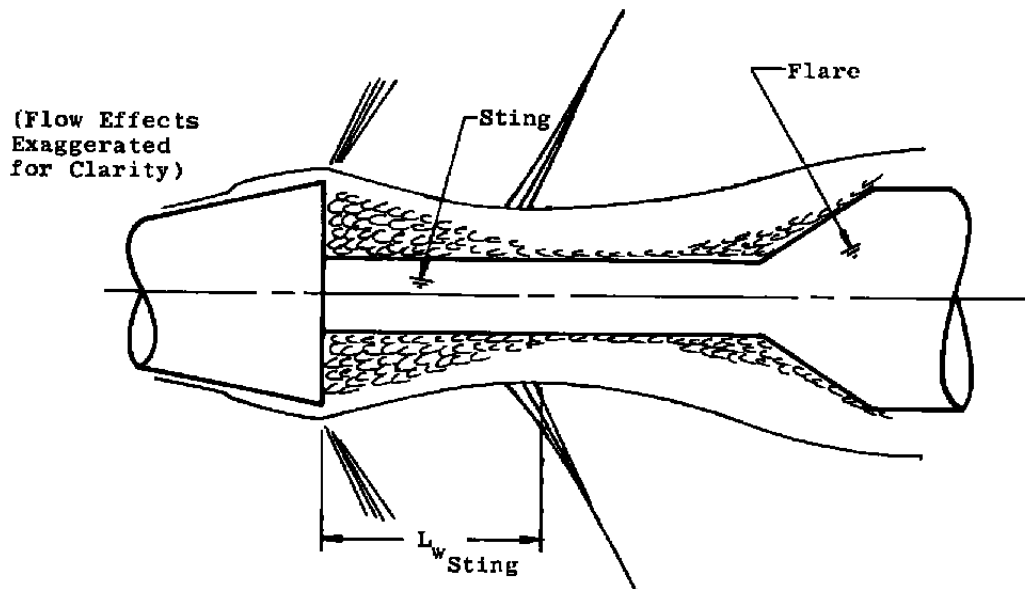
b. Influence of a sting in the wake

Figure 1. Wake formation with and without a sting
support (M > 1).

II.   Statement of the Problem

Considering the previous work on the subject of sting interference, there are still significant gaps in the available data. Many questions remain to be answered in relation to assessing the magnitude of possible interference effects on the testing of an arbitrary model at any given flow condition. Some pertinent questions are:

1.   What are minimal interference sting configurations as opposed to configurations producing substantial interference?

2.   Are there any critical sting geometry parameter limits that distinguish between significant and negligible interference? If so, how can they be delineated?

3.   Since the use of base pressure as an interference indicator is not often representative of interference on other measurements, how can base pressure interference data be correlated to other measurements?

The purpose of this investigation is to provide a better insight into sting interference effects on static and dynamic measurements for a blunt slender cone in transonic flow. The overall intent of this study is to:

1.   Discuss some of the causes of sting interference in regard to similar models at transonic speeds.

2. Identify the relative interference effects caused by various sting geometries.

3. Establish some guidelines for predicting sting interference effects on the measurements of dynamic stability derivatives.

4. Provide test results which will contribute to the search for an overall solution to minimize support interference.

An analysis of sting interference effects at transonic Mach numbers on general model configurations is beyond the scope of this investigation, but the results of this study should be applicable to most slender, flat base cones and nose-cylinder configurations without boattail in the same Mach number and Reynolds number range. All flow conditions presented in this study are limited to flow conditions that produce a turbulent boundary layer over the aft portion of the model. In addition, emphasis will be placed on the determination of sting length interference effects.

CHAPTER II

CAUSES OF INTERFERENCE

This chapter will discuss the various effects of
sting interference caused solely by aerodynamic phenomena.
However, interference caused by the nongeometric properties
of the sting, such as vibration transmission, heat con-
duction and balance imperfections, as well as wind tunnel
wall interference and tunnel flow anomalies, may also
influence the model aerodynamic measurements. For
simplicity, a discussion of these effects will not be pre-
sented in this chapter, but some of these effects on the
data obtained during this investigation will be addressed
in Chapter III. Since aerodynamic interference caused by
any support system is primarily a function of the geometry
of the model and sting, and of the flow conditions, the
bulk of this chapter will be devoted to analyzing these two
factors.

As a starting point for this discussion, consider
the typical sting support configuration shown in Fig. 2.
In addition to the model geometry, five parameters are of
significance: D, D_S, L_S, D_f, and θ_S. It is often con-
venient to nondimensionalize the characteristic lengths
with respect to the model base diameter to obtain the
ratios D_S/D, L_S/D and D_f/D. The sting diameter ratio
(D_S/D) defines the effect of the cylindrical sting. The

8

Model
Geometry

Cylindrical
Sting

Conical
Flare

D_f

θ_S

D

D_S

L_S
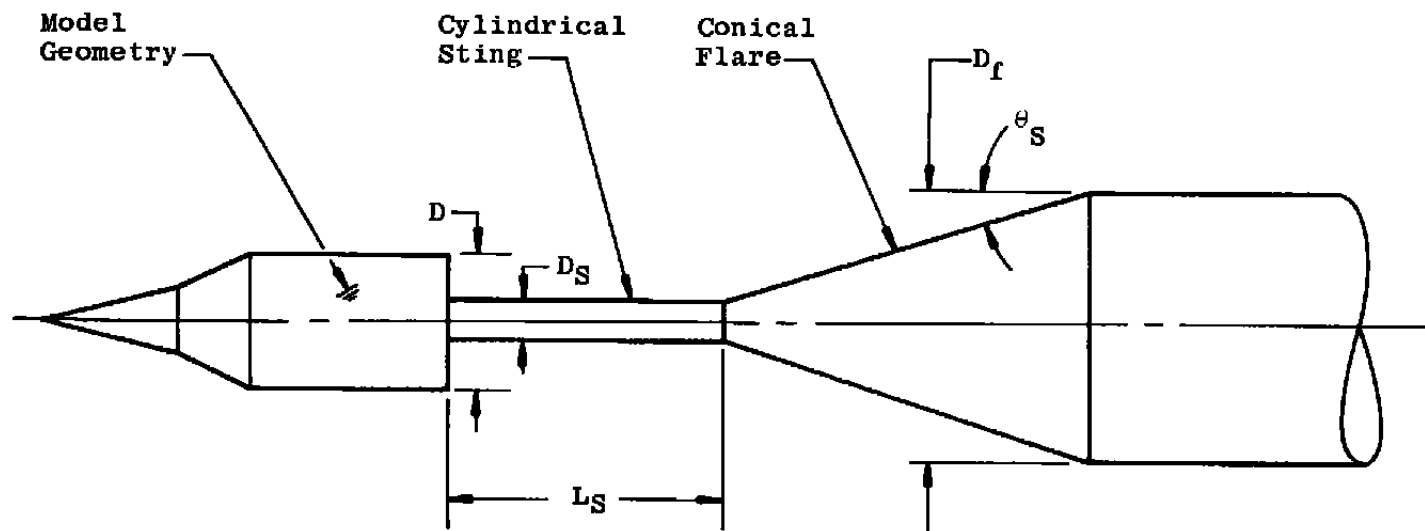
Useful Sting
Parameters:

L_S/D D_S/D D_f/D θ_S

————————— (Sting) Flare Angle

————————— (Sting) Flare Diameter Ratio

————————— (Cylindrical) Sting Diameter Ratio

————————— Sting Length Ratio

Figure 2.   Geometric variables of a typical rear-mounted sting configuration.

conical flare is defined by the sting length ratio (L_S/D),
flare diameter ratio (D_f/D), and the flare angle, θ_S. A
minimal interference sting configuration would thus embody
a maximized L_S/D, with the remaining parameters minimized
as much as possible. However, overall tunnel consider-
ations, instrumentation, structural and control
requirements usually govern these limits.

In analyzing the geometric properties of the sting,
it is evident that aerodynamic support interference can be
divided into two effects: those attributed to the presence
of the cylindrical sting, and those caused by the conical
flare. For the case of the typical sting, the effects of
both are present (Fig. 3), although one effect may be
dominant, depending on the geometry.

First, consider the interference-free model flow
field in Fig. 3a. An illustration of the variation of the
pitch-damping derivatives and base pressure ratio for this
case is shown in Fig. 4.[1] At Mach numbers less than 0.8,
the flow around the model is completely subsonic, and both
the damping derivatives and base pressure are influenced
primarily by the base flow separation and the properties of
the downstream wake. As the Mach number increases into the

[1]Although these data were obtained with the model
mounted on a sting and are not completely free of inter-
ference, it was concluded from this investigation that, for
this particular set of data, interference effects are
negligible. Thus, the data in Fig. 4 will be considered
representative of interference-free data.

a. Free wake

b. Cylindrical sting only

c. Conical flare only

d. Cylindrical sting and conical flare
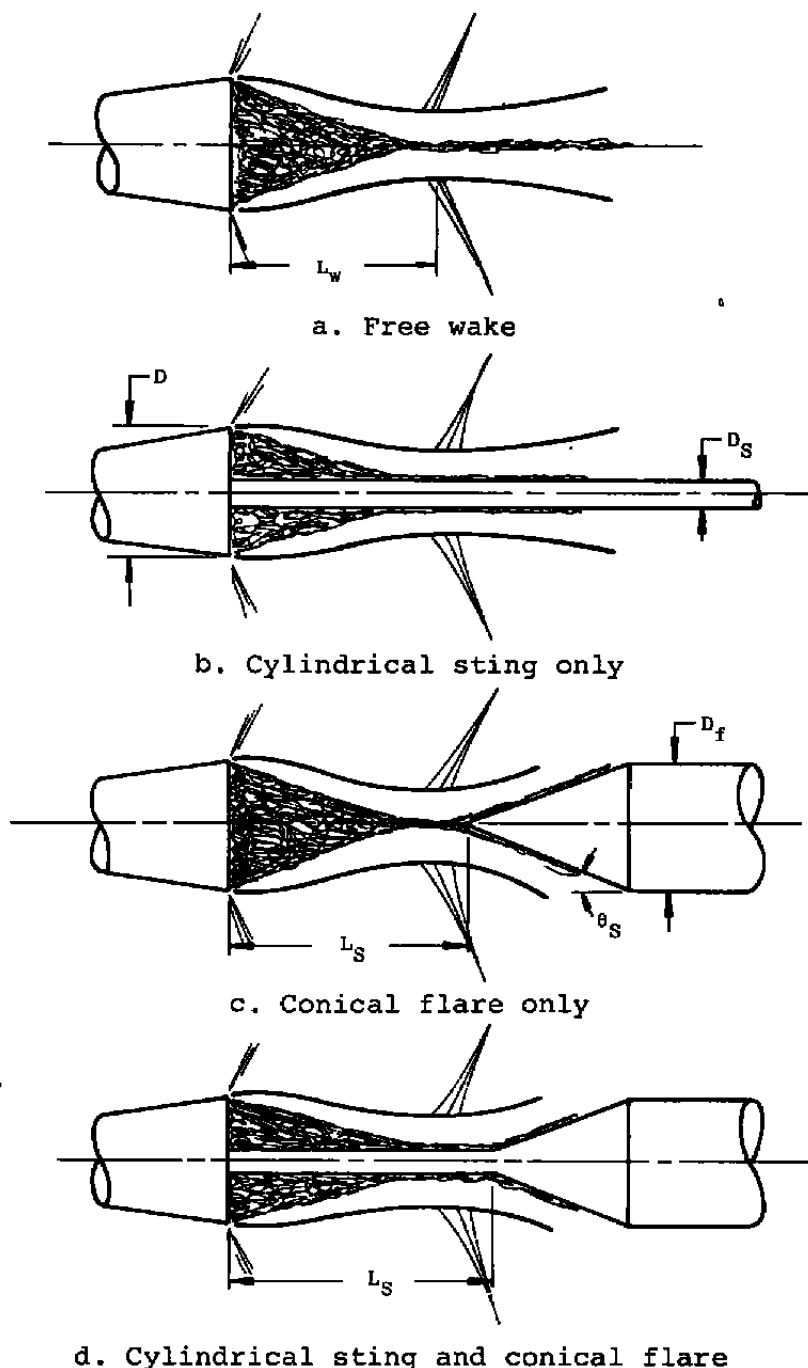
Figure 3.   Combinations of cylindrical sting and conical
flare interference configurations.

11

7-deg Cone, 15-percent Bluntness　　　Turbulent Boundary Layer
Oscillation Frequency ≅ 5.3 Hz　　　$\alpha = 0$, $\theta = \pm 1$ deg, $L_S/D \geqslant 3$
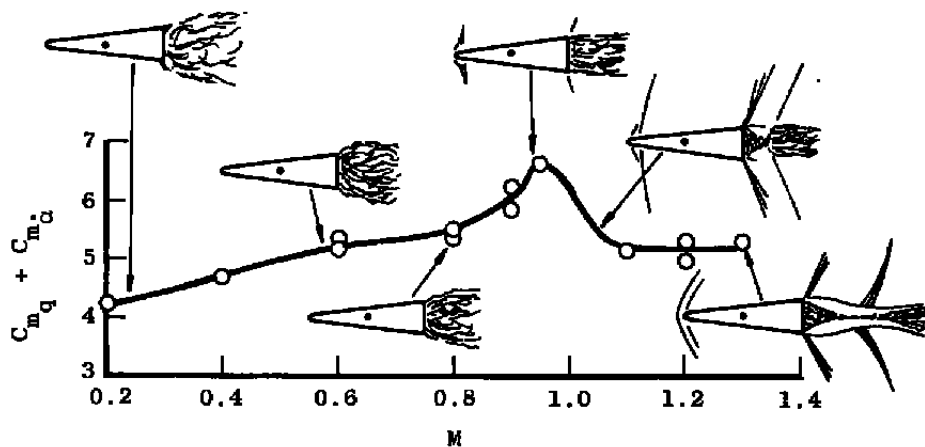
a. Pitch-damping derivatives
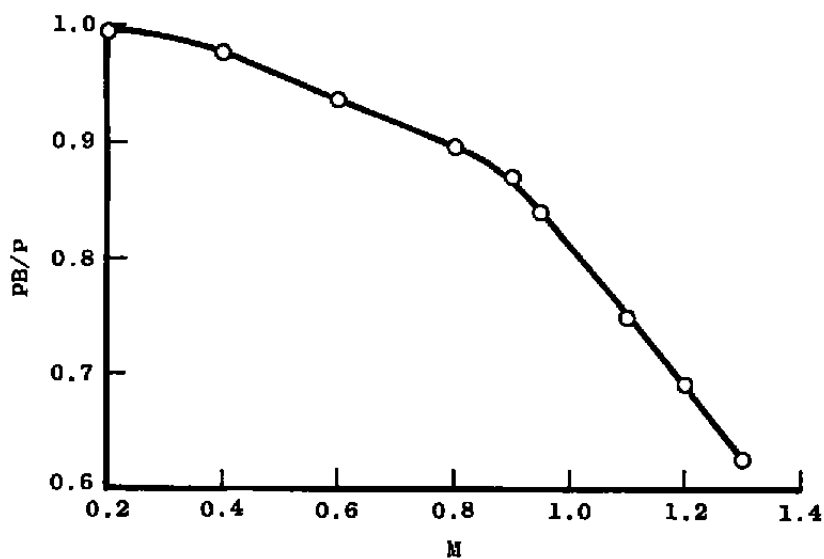
b. Base pressure

Figure 4.　Variation of pitch-damping derivatives and base
pressure over the subsonic and transonic Mach
number range [16, 25].

12

range $0.8 < M \leq 0.95$, a shock wave forms near the model
nose, and an expansion fan forms at the base. The Mach
number at which the base pressure ratio changes abruptly in
Fig. 4b probably indicates the initial formation of the
base expansion fan. In this Mach number range the nose
shock wave is completely attached, which results in an
increase in overall model damping as the Mach number
increases. Moreover, as the Mach number is increased above
$M = 0.95$, the nose shock wave detaches, resulting in a loss
of nose-induced damping. It can thus be inferred that at
Mach numbers where the nose shock is detached the model
damping characteristics are governed primarily by the flow
over the shoulder of the model (the expansion fan) and the
flow in the model base region. However, the damping
induced by the nose is also significant for this case. In
contrast, at subsonic Mach numbers where no shock is
present, the nose-induced damping is negligible (a con-
clusion proposed by Ericcson [10]).

Next, consider the presence of a cylindrical sting
(Fig. 3b). It is obvious that for any sting diameter ratio
greater than zero, the base flow field will be affected.
By comparing theoretical and experimental data, Chapman
[11] concluded that for a fixed Mach number and Reynolds
number, an increase in the support diameter brings about
two different effects. First, the wake thickness was found
to increase slightly as the support diameter was increased
from zero to D (the base diameter), and based on this

observation, an inviscid method of characteristics analysis predicted that a lower base pressure would result. The second effect resulting from an increase in the support diameter is that the boundary layer thickness ratio $\delta/(D-D_S)$ is increased, thereby tending to increase the base pressure. These two effects therefore oppose each other. Chapman stated that the first effect would be expected to predominate for small values of D_S/D, and that the second effect must predominate at values of D_S/D close to unity. The experimental data at Mach numbers 1.5 to 2.9 presented by Chapman supported these assumptions, and showed that as D_S/D increased from 0.3 to 0.85, the base pressure decreased smoothly (the first effect). For values of D_S/D greater than 0.85, the base pressure increased sharply (the second effect).

Data obtained by Lee and Summers [4] at subsonic and transonic Mach numbers with both a strut and sting support (Fig. 5) were also found to be in agreement with Chapman's supersonic data. In Fig. 5, the base drag coefficient C_{D_B} (which in this case is equal to $-(PB-P)/Q$) at various Mach numbers from 0.6 to 1.4 is shown to increase (corresponding to a measured decrease in base pressure) as D_S/D increases. This trend is more evident at the higher Mach numbers. From Fig. 5, it is evident that Chapman's first effect (increasing wake thickness decreases base pressure) predominates at least up to values of $D_S/D = 0.75$, especially at Mach numbers greater than 1.0.

14
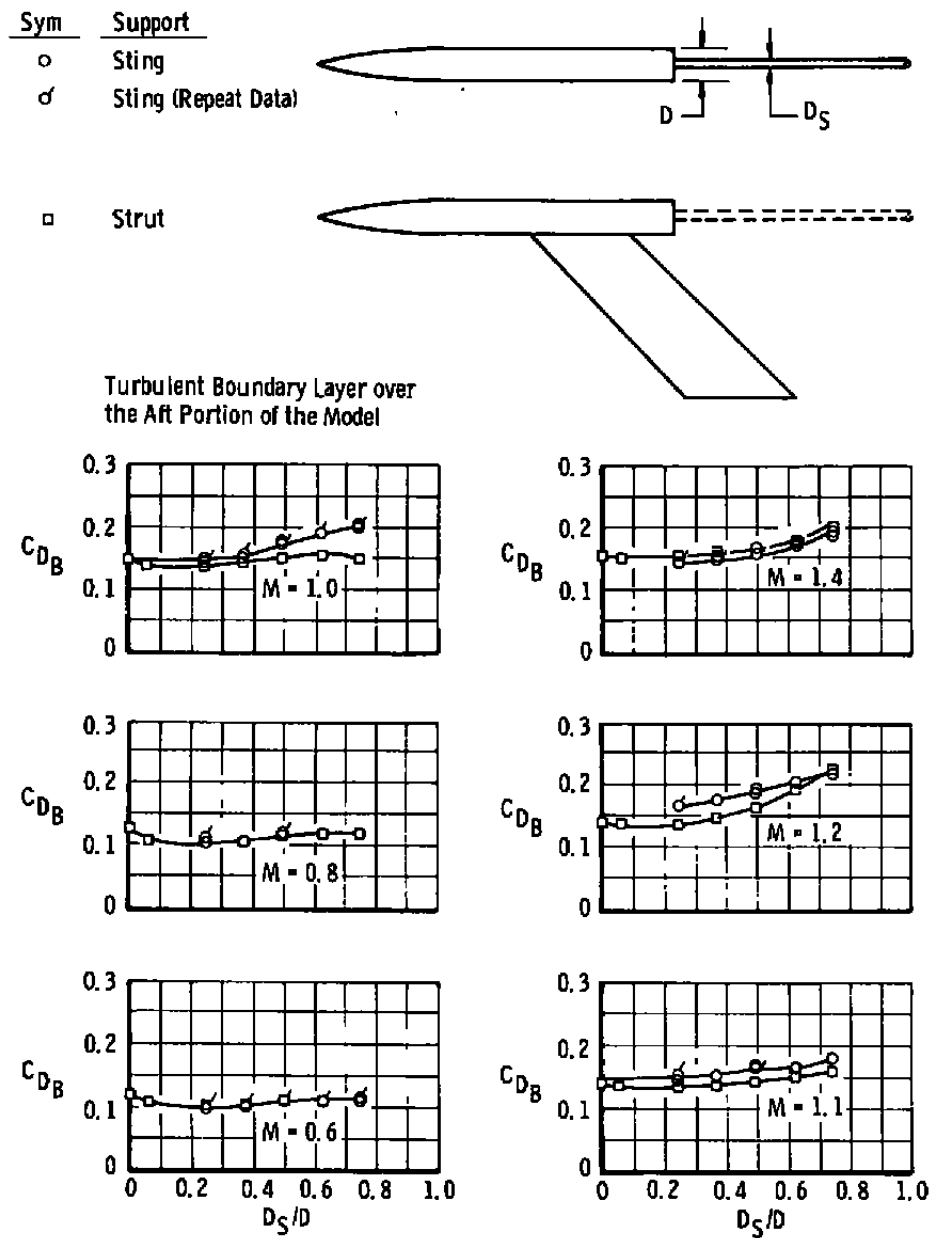
Figure 5. Base drag as a function of sting diameter ratio [4].

15

An interesting analogy can be made between two-dimensional airfoil sections with trailing-edge splitter plates (Fig. 6) and bodies of revolution mounted on three-dimensional sting configurations with a small, but finite, sting diameter ratio. Base pressure data obtained by Nash, et al. [12] on a flat-trailing edge airfoil section with various length splitter plates are shown as a function of Mach number in Fig. 6. The airfoil section accompanied by the splitter plate may be viewed as having an "equivalent" D_S/D analogous to the actual sting diameter ratio possessed by a similar three-dimensional model-sting configuration. For this particular analogy, the parameter ℓ/D should not be confused with the sting length ratio L_S/D. The parameter ℓ/D is only an indicator of how "infinite" the splitter plate is, and does not represent the concept of sting length interference effects. All models with the splitter plate in Fig. 6 have an "equivalent" D_S/D of 0.067. This is an extremely small value as compared to most three-dimensional model-sting configurations which normally have a D_S/D of 0.2 or greater. The base pressure coefficient C_{P_B} is found to be influenced highly by the presence of the splitter plate at Mach numbers less than 1.0. However, at Mach numbers greater than 1.0, C_{P_B} is relatively unaffected by the presence of the plate, with the value of C_{P_B} for the basic model being very near the value of C_{P_B} for the backward-facing step.
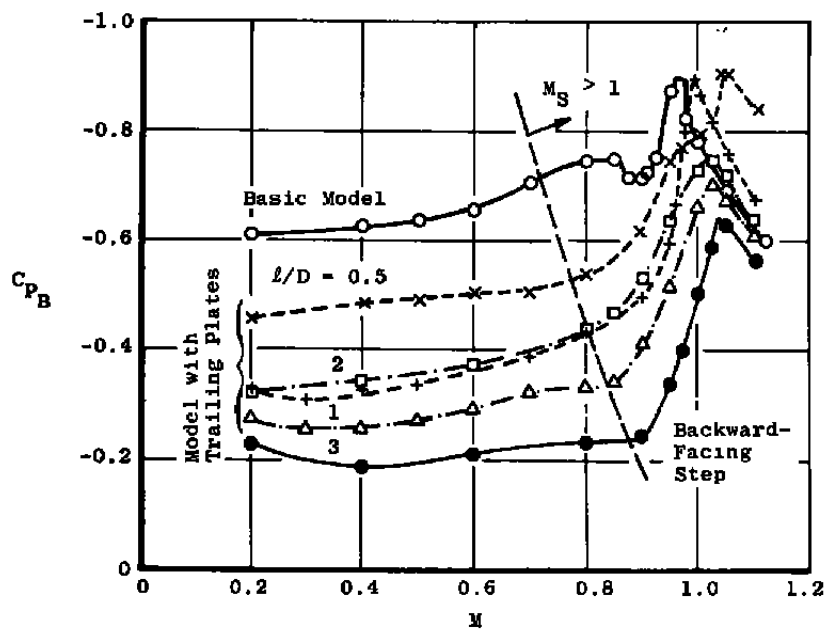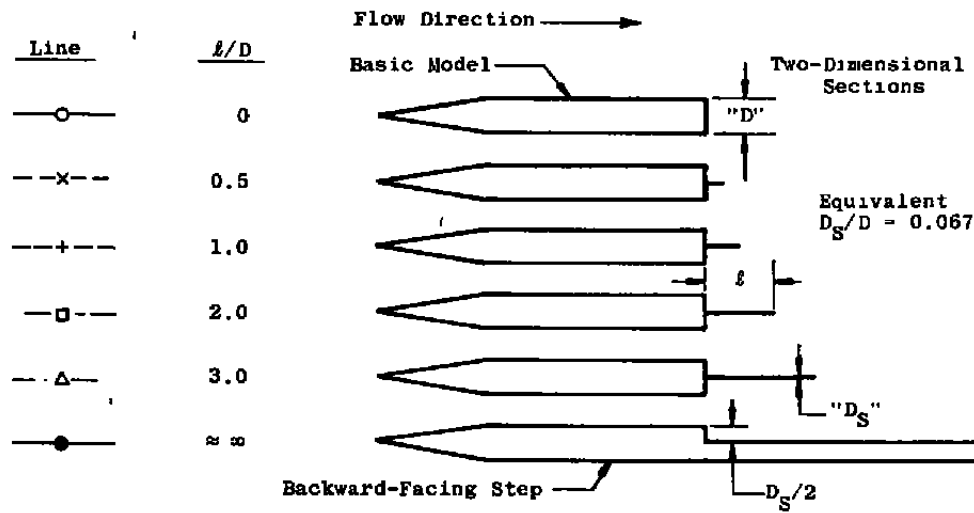
Figure 6.   Base pressure coefficients on various two-
dimensional airfoil sections with trailing
plates [12].

The effects shown in Fig. 6 for the two-dimensional section are due primarily to the vortex strength and shedding frequency caused by the trailing edge of the airfoil. Although vorticity effects are not usually as pronounced in a corresponding steady three-dimensional flow, they are significant for an oscillating three-dimensional model that produces an oscillatory base flow. Using this analogy and assuming that the two-dimensional results of Fig. 6 exemplify an oscillating three-dimensional model sting configuration, it appears likely that the interference effects of a cylindrical sting support are primarily a subsonic phenomenon. This is quite different from the previously discussed steady flow results obtained by Lee and Summers [4], which indicated that cylindrical sting interference is more noticeable at Mach numbers near and greater than 1.0.

Now that the interference effects of a cylindrical sting alone have been discussed, the effects of sting length will be considered. In this discussion, sting length interference effects refer only to the effects attributed to the presence of an abrupt geometric contour aft of the model, as shown in Figs. 3c and 3d, page 11. Consider the conical flare only (Fig. 3c), which is a good starting point for the study of "length" interference of a conical flare. It will be assumed that the flare diameter ratio D_f/D is on the order of unity, and the flare angle θ_s is in the range of 3 deg < θ_s < 20 deg. Geometrically,

it appears evident that L_S/D, D_f/D, and θ_S are undoubtedly functions of the resulting magnitude of interference caused by the flare. From this observation it can be assumed that the presence of the flare will have no influence on the flow field surrounding the model if the flare is located downstream at some distance L_{cr} (the critical length) from the model base. It can also be assumed that L_{cr} is greater than the distance from the base of the model to the wake neck location (L_w) for a free wake (Fig. 3a, page 11). At distances greater than or equal to L_{cr}, disturbances caused by the flare will not propagate into the model base region. Thus, the concept of critical length can be established as the minimum length aft of the model that a flare may be located without affecting the measurable aerodynamics of the model. For convenience, the critical length is usually non-dimensionalized as the critical sting length ratio, L_{cr}/D.

Now that both of the major causes of sting inter-ference (namely, the cylindrical sting and the conical flare) have been examined individually, the typical sting in Fig. 3d can be considered. Unless otherwise noted in the discussions to follow, any mention of interference effects caused by the presence of a cylindrical sting will be referred to as "sting diameter effects." Likewise, the presence of a conical flare will be referred to as "sting length effects." As stated previously in this section, for a typical sting configuration having both a cylindrical

sting and a conical flare, both sting length and diameter effects are present, although it is possible that either effect may dominate. Usually, one effect is traded for the other. For example, as L_S/D decreases, sting length effects dominate (the presence of the flare overshadows the presence of the cylindrical sting). Conversely, as L_S/D increases, sting diameter effects dominate. However, in instances where L_S/D tends toward zero and reattachment occurs downstream of the sloped surface of the flare, the flare affects the flow field surrounding the model in much the same way as a large diameter cylindrical sting (compare Figs. 7a, b, and c). Pitching the sting configurations in Figs. 7a, b, and c to a substantial angle of attack would appear to diminish sting length effects, but accent sting diameter effects (compare Figs. 7d, e, and f). This is due to the large crossflows in the wake region resulting from the large diameter afterbodies in Figs. 7e and f relative to Fig. 7d. An additional result of the large wake crossflows is the forward movement of the leeward flow separation point.

With the exception of the previously presented two-dimensional analogy, the interference effects discussed so far have dealt with the testing of static models. Statically, models are tested without any movement of the model relative to the sting, excluding possible balance deflections. However, for a dynamic test, aerodynamic measurements are based on the motion of the model relative

20
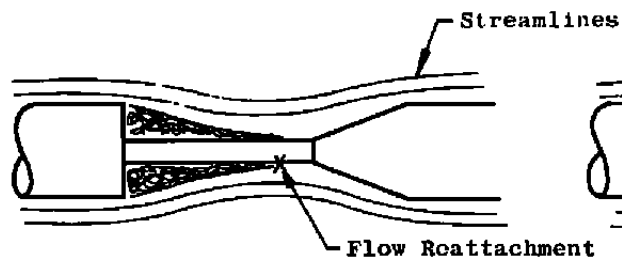
a. Long sting length,
   α = 0
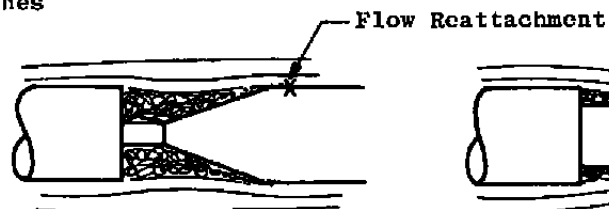
b. Short sting length,
   α = 0
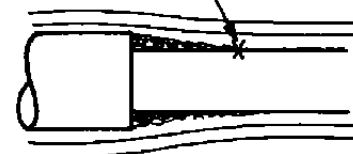
c. Excessive sting diameter,
   α = 0
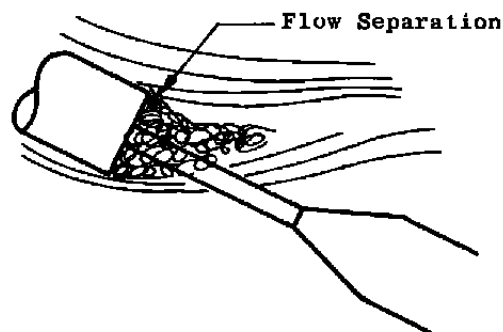
d. Long sting length,
   α >> 0
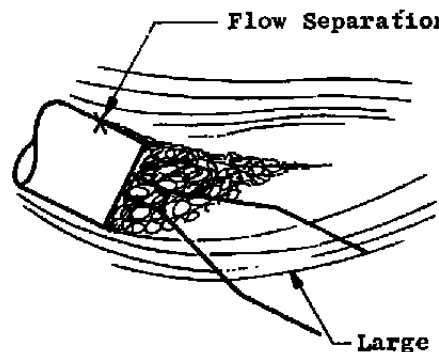
e. Short sting length,
   α >> 0
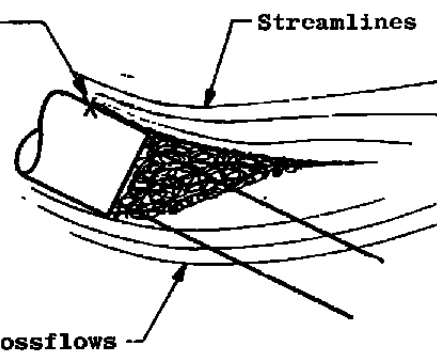
f. Excessive sting diameter,
   α >> 0

Figure 7. Similarity between short sting lengths and excessive sting diameter interference.

to the sting. In addition, it may be necessary to conduct
a dynamic test with a larger sting diameter than would be
required for a static test to retain sting rigidity. Many
types of dynamic tests are commonly performed in wind
tunnels, such as Magnus, three-degrees of freedom, and
planar motion, but the present discussion will be limited
only to planar motion with special reference to pitch-
damping. This discussion is also complemented by the
significant amounts of sting interference data available
based on this type of dynamic measurement (refer to
Bibliography).

As opposed to static force and moment tests, where
the flow field around the model can be considered non-
varying, a model undergoing pitch oscillation motion
relative to the sting is subjected to a base-plunging
effect. This is shown in Fig. 8. This effect would be
minimized if the motion of the model was constrained to
rotate about a pivot axis located at the base. However,
few (if any) actual flight vehicles have a center of
gravity location coincident with this pivot axis because of
the high degree of static instability that would result.
If the base plunging is too severe, the sting may influence
the flow separation point on the aft portion of the model.
This would provide a means by which downstream influence
caused by the sting would propagate up onto the model.
Thus, significant interference on dynamic measurements may
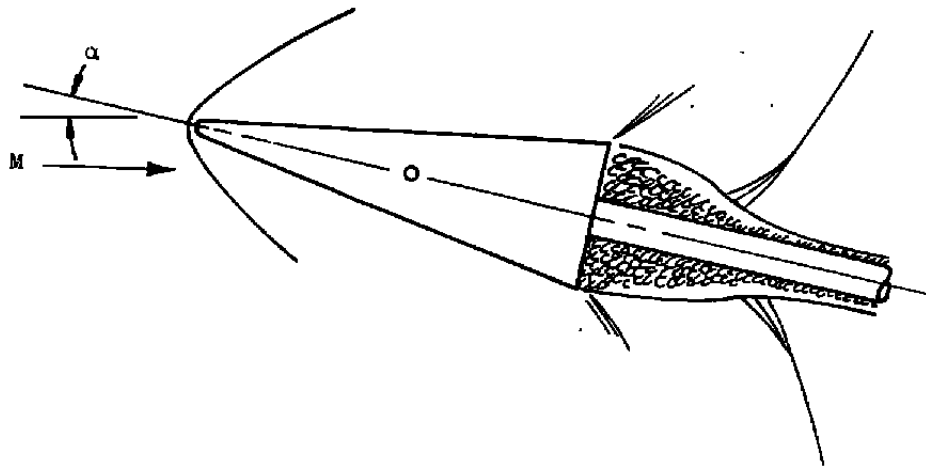
a. Static sting interference
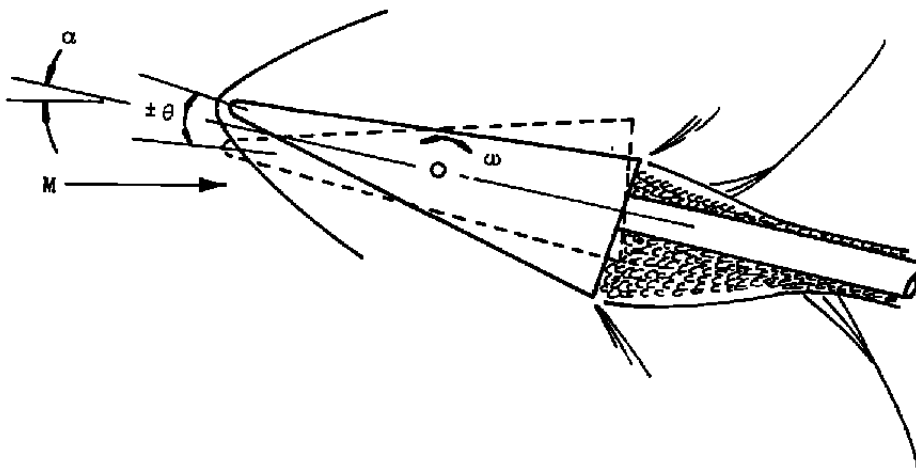
b. Dynamic sting interference

Figure 8. Difference between sting interference on static
and dynamic models.

be possible even though interference on the static measurements may be negligible.

In an attempt to analyze the reasons for dynamic interference to be more pronounced than static interference, Reding and Ericcson [13] proposed that dynamic interference was influenced significantly by a flow field time lag due to the oscillation of the model. This time lag effect was characterized by the finite convection speed downstream to the wake neck and the following upstream convection through the wake recirculation region. Reference [13] concluded that any sting configuration that allows base interference effects to be communicated forward of the base and affect the longitudinal loads would be subjected to dynamic sting interference.

CHAPTER III

APPARATUS

I. Wind Tunnel

The Aerodynamic Wind Tunnel (4T) is a closed-loop,
continuous flow, variable-density tunnel in which the Mach
number can be varied from 0.1 to 1.3 and can be set at
discrete Mach numbers of 1.6 and 2.0 by placing nozzle
inserts over the permanent sonic nozzle. At all Mach
numbers, the stagnation pressure can be varied from 400 to
3,400 psfa. The test section is 4-ft square and 12.5-ft
long with perforated, variable porosity (0.5- to 10-percent
open) walls. It is completely enclosed in a plenum chamber
from which the air can be evacuated, allowing part of the
tunnel airflow to be removed through the perforated walls
of the test section. A more complete description of the
tunnel may be found in Ref. [14].

II. Model

The model was a flat, open base, 7-deg half-angle
cone with a nose bluntness ratio (nose diameter to base
diameter) of 15 percent. The moment reference axis was
located on the model pivot axis at 60.9 percent of the
model length aft of the model nose on the cone centerline.
The center of gravity of the model was chosen to be

representative of a typical conical reentry vehicle, and
was also coincident with the model pivot axis. The model
was constructed of stainless steel and had a total weight
of 30.4 lbs and a moment of inertia about the pivot axis of
0.408 slug-ft^2. The surface finish was a nominal 32 rms
(32 $\sqrt{}$). A sketch of the model and external dimensions is
shown in Fig. 9.

III. Test Mechanism and Interference Hardware

The von Karman Facility (VKF) 1.C Forced Oscil-
lation Test Mechanism (Fig. 10) was used to measure the
various static and dynamic pitching moments used in the
calculation of the pitch-damping derivatives $C_{m_q} + C_{m_{\dot\alpha}}$,
the pitching moment slope C_{m_α}, and the static pitching
moment C_m. This mechanism utilizes a cross flexure pivot,
an electric shaker motor and a one-component moment beam
instrumented with strain gages to measure a sinusoidal
forcing moment produced by the shaker motor. The motor is
coupled to the moment beam by means of a connecting rod and
flexural linkage. The flexural linkage converts the trans-
lational force to a moment to oscillate the model at
amplitudes up to ±3 deg (depending on the balance flexure)
and frequencies from 2 to 8 Hz. The cross flexures, which
are instrumented to measure the pitch/yaw displacement,
support the model loads and provide the restoring moment to
cancel the inertia moment when the system is operating at
its natural frequency. The moment beam is not subjected to

Moment Reference
Point (Pivot Axis)

7 deg

0.600 Sph Rad

8.000
Diam (D)

17.206

28.246

All Dimensions in Inches
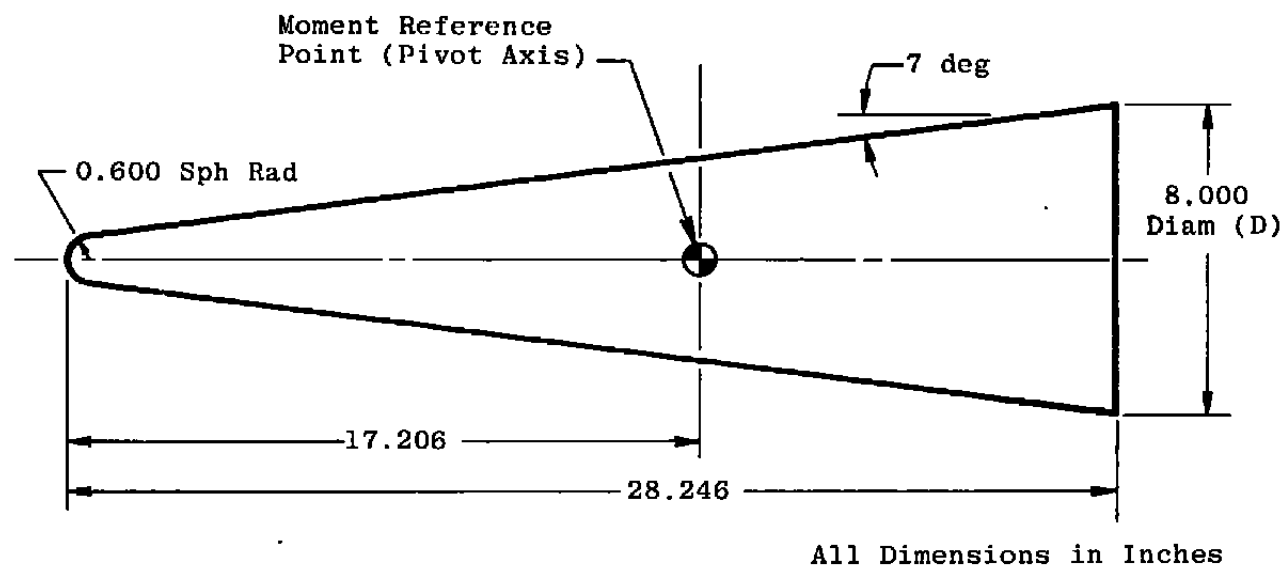
Figure 9.   Model details.
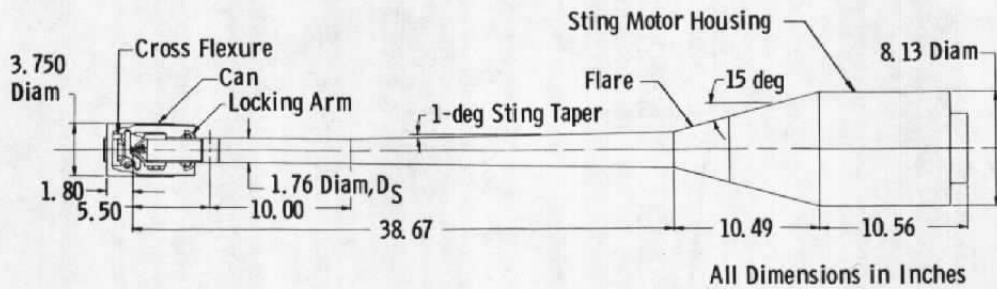
a. Forced oscillation test mechanism
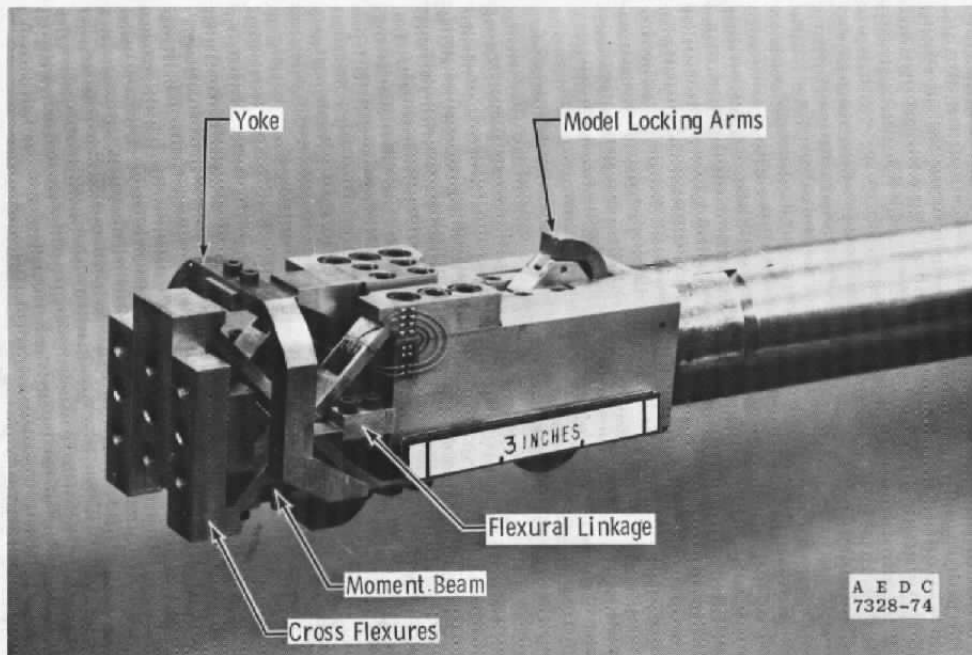
b. Close-up photograph of balance

Figure 10.   Test mechanism.

the static loads and can be made as sensitive as required
for the dynamic measurements. A pneumatic- and spring-
operated locking device is provided to hold the model
during tunnel start-up and shut-down.

The cross flexure pivot, moment beam, and flexural
linkage assembly is supported by a long, slender,
cylindrical sting with a 1-deg taper. The sting is instru-
mented with strain gages to measure the static and
oscillatory deflections of the sting in both the pitch
and yaw plane for use in correcting the data for sting
oscillation effects. These sting gages are located at
approximately 15 in. aft of the cross flexure pivot.

The model, when mounted to the test mechanism, had
an effective L_S/D of 3.4 and an effective D_S/D at the model
base of 0.22. The sting length was effectively shortened
by positioning a conical flare (Fig. 11) at 1.0, 1.5, 2.0,
2.5, 3.0, or 3.3 model diameters to the rear of the model
base along the sting. A means to vary the sting diameter
was not available. The flare was mounted to the motor
housing without touching the sting forward of the motor
housing. This mounting eliminated the possibility of the
flare changing the sting frequency characteristics or model
tare damping.

The test mechanism and interference hardware used
in this investigation were also used in the tests reported
in Refs. [2] and [3]. A sketch of the model installation is

All Dimensions in Inches

Tunnel Boom (Typical)

Clutchface Centerline
Sting Motor Housing
(See Fig. 10)

Steel Fairing Attached to Sting

8.0
(L_S)

15 deg (θ_S)

1.76 Diam (D_S)

8.0 Diam

8.5 Diam

Attachment Lugs

76.9

a. $L_S/D = 1.0$

26.4
(L_S)

15 deg (θ_S)

1.76 Diam (D_S)

Flare

b. $L_S/D = 3.3$
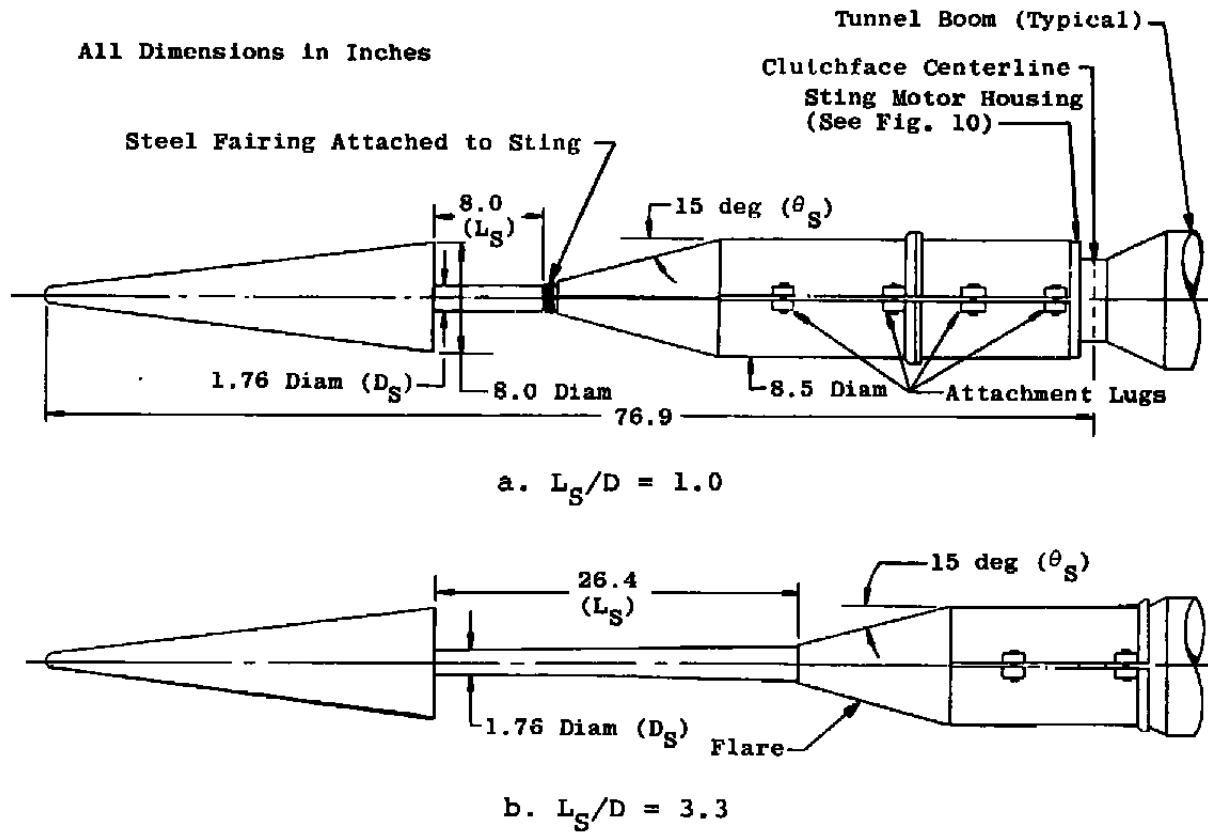
Figure 11.   Details of model support configurations.

presented in Fig. 12. A photograph in Fig. 13 shows a typical model-sting configuration in the test section.

IV. Instrumentation

Forced Oscillation

The forced-oscillation instrumentation [15] utilizes an electronic analog system with precision electronics. The control, monitor, and data acquisition instrumentation are contained in a portable console. The control instrumentation provides a system which can vary the oscillation amplitude of the model within the flexure limits. The oscillation amplitude is controlled by an electronic feedback loop which permits testing of both dynamically stable and unstable configurations. Data are normally obtained at or near the natural frequency of the model-flexure system; however, electronic resolvers in the instrumentation permit data to be obtained off resonance.

All gages are excited by d-c voltage and outputs are increased to optimum values by d-c amplifiers. Typical balance outputs from an oscillating model are composed of oscillatory components (OC) superimposed on static components (SC). These components are separated by band-pass and lowpass filters. The SC outputs are used to calculate the static moment coefficients (C_m) and static sting deflections (used in the calculation of model angle of attack). The OC outputs are input to the resolver instrumentation and precise frequency measuring

31

Sting Configuration Shown
Without Movable Conical
Flare Attached, $L_S/D = 3.4$
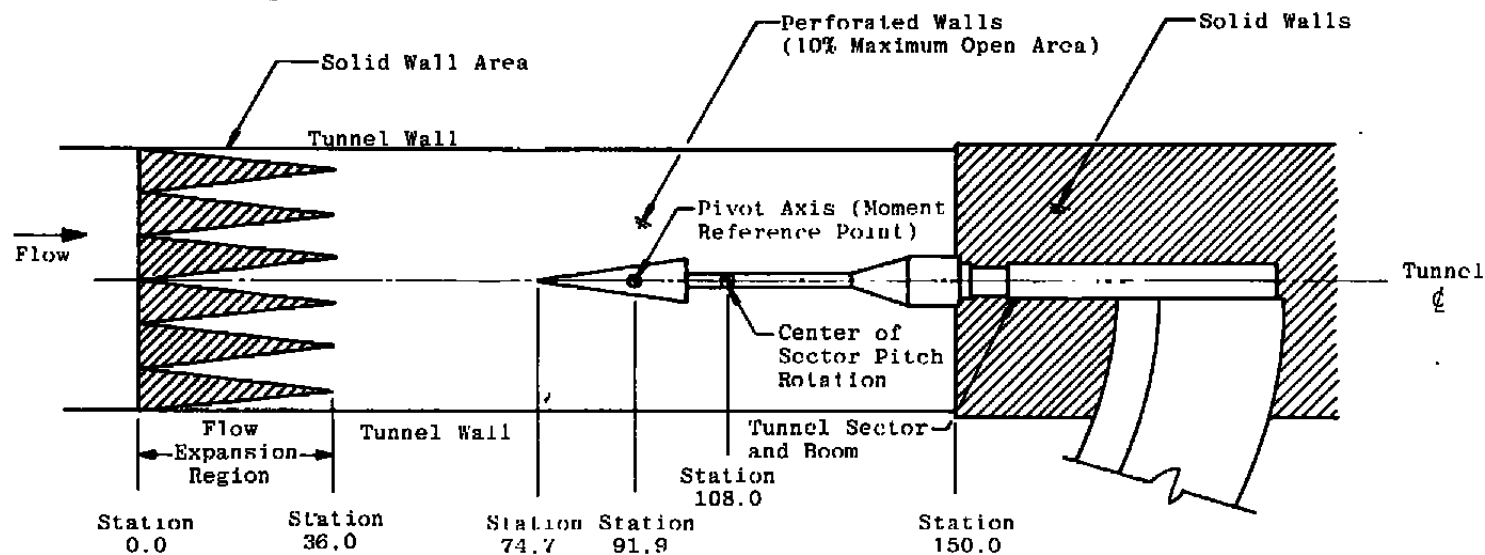
Figure 12.   Sketch of model installation.
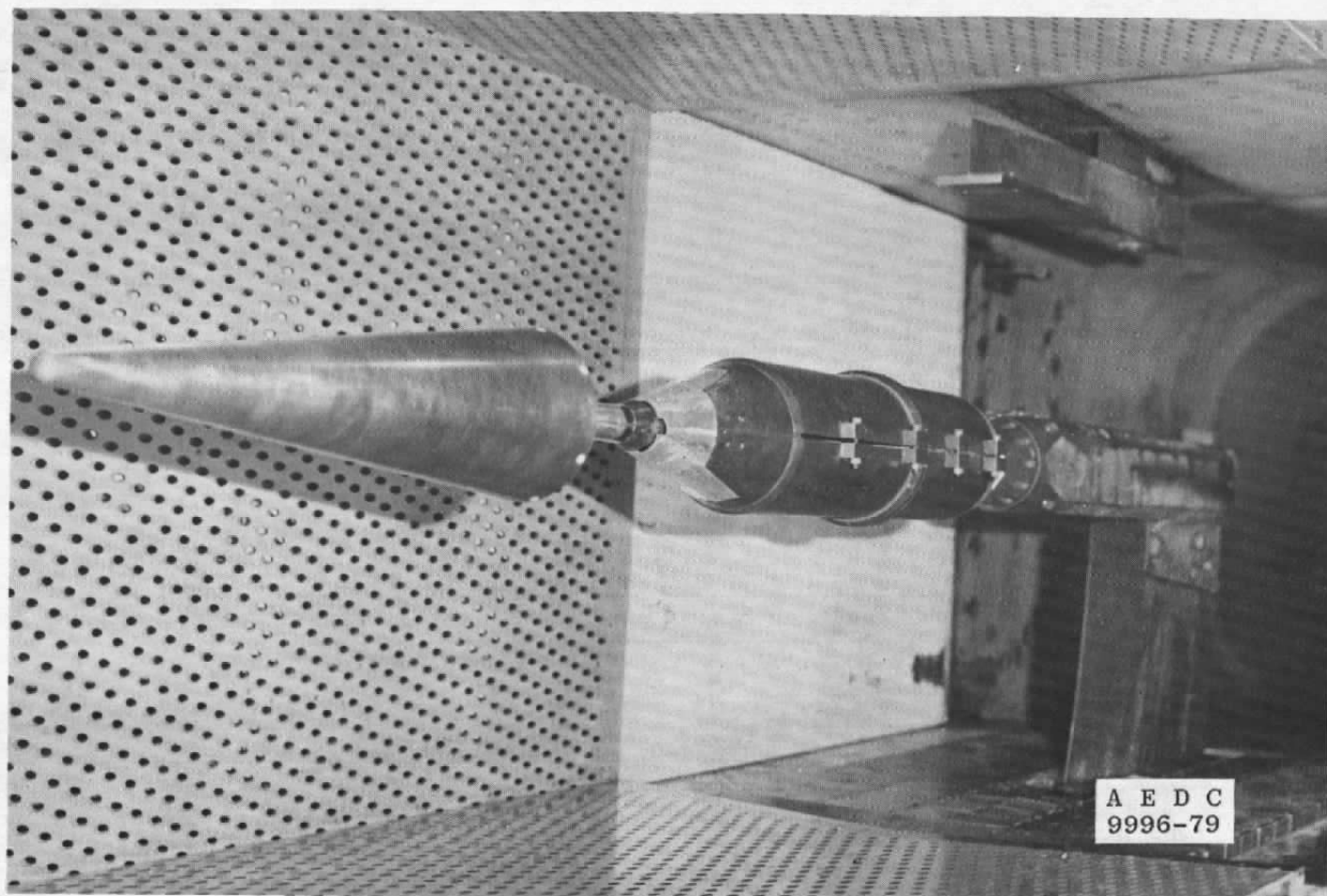
Figure 13.   Photograph of model installation, L_S/D = 1.0.

instrumentation for calculating the dynamic moment coefficients ($C_{m_q} + C_{m_{\dot\alpha}}$ and C_{m_α}). The resolvers utilize very accurate electronic analog devices to process the OC signals and output d-c voltages. The output d-c voltages are proportional to the square of the oscillation amplitude, the in-phase and quadrature (90 deg out-of-phase) balance forcing torque components and the in-phase and quadrature sting moment components. These outputs are converted to digital signals by an analog-to-digital converter for transmission to the computer system for data reduction.

Model Base Pressure

Model base pressure was measured with a Sunstrand®
(Kistler) 314D Servo pressure transducer located on the tunnel plenum chamber wall. The location of the orifice with respect to the model and sting is shown in Fig. 14.

This transducer was intended to measure the average base pressure, and was not suitable to measure high-frequency pressure changes. Data from Ref. [2] showed that the base pressure is essentially constant for this model at the same frequency of oscillation at supersonic Mach numbers. Based on this data, it was assumed that the base pressure for this test was also essentially constant. However, no additional probing in the base region was performed to verify this assumption.
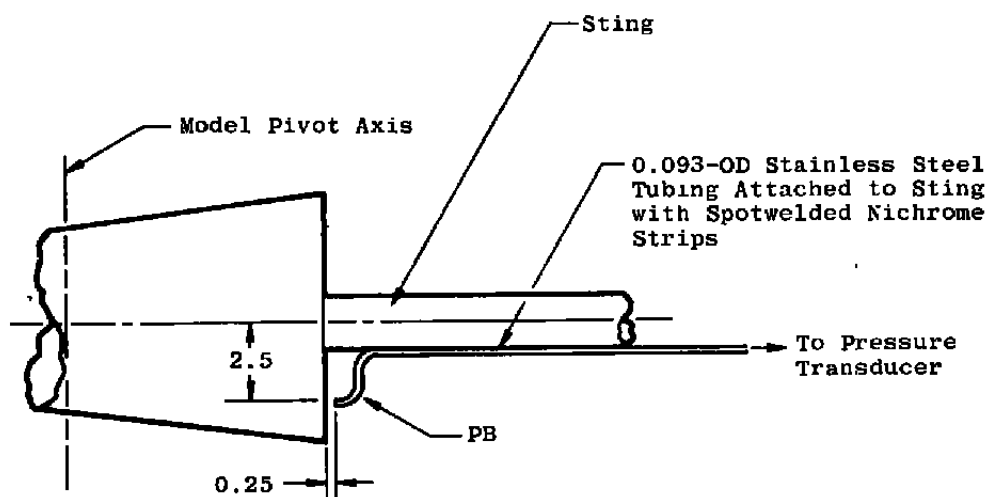
Figure 14. Location of base pressure orifice.

CHAPTER IV

EXPERIMENTAL TECHNIQUE

I. Test Conditions and Procedures

A summary of the nominal test conditions for the
data presented in this investigation is listed in Table 1.
A list of all conditions tested, ranging from Mach number
0.2 to 1.3, and the complete test summary, may be found in
the Test Summary Report [16].

After establishing tunnel conditions and model
attitude, the model was unlocked and brought to an oscil-
lation amplitude of ±1 deg by using the forced oscillation
control system. The frequency of oscillation was a nominal
5.3 Hz. At each angle of attack, generally two data points
were taken. Data were obtained over a 60-sec time interval
for each data point, at a rate of approximately 200 samples
per second.

II. Data Reduction

The time-varying balance and sting gage signals,
and steady-state model attitude and base pressure measure-
ments were transmitted to a DEC-10 System Computer.
Average values of the balance and sting gage outputs were
calculated by the computer and used to calculate the
dynamic derivatives.

36

Table 1. Test Conditions

M	PT (psfa)	TT (°R)	Q (psf)	P (psf)	V (ft/sec)	$\omega D/2V$ (radians)	$Re_D \times 10^{-6}$
0.2	400	554	11	389	230	0.0483	0.16
0.2	820	550	·22	797	230	0.0483	0.33
0.2	2,000	556	54	1,945	232	0.0478	0.78
0.2	3,200	586	87	3,112	236	0.0470	1.20
0.4	870	553	87	779	454	0.0244	0.67
0.6	1,630*	569	322	1,278	678	0.0164	1.66
0.8	1,320	555	388	866	870	0.0128	1.66
0.9	1,260*	556	422	745	965	0.0115	1.66
0.95	800	550	283	448	1,005	0.0110	1.09
0.95	1,020	554	360	571	1,009	0.0110	1.38
0.95	1,220	556	431	683	1,011	0.0110	1.64
0.95	1,600	560	565	895	1,014	0.0109	2.13
0.95	2,200	567	778	1,231	1,021	0.0109	2.88
0.95	2,800	578	990	1,567	1,030	0.0109	3.58
1.10	1,200*	555	476	562	1,140	0.0097	1.67
1.20	1,200	556	499	495	1,222	0.0091	1.68
1.30	1,300*	556	555	469	1,299	0.0085	1.82
1.30	1,600	568	683	577	1,313	0.0085	2.17
1.30	2,200	578	939	794	1,325	0.0084	2.92
1.30	2,560	588	1,093	924	1,336	0.0083	3.33
1.30	2,700	591	1,153	974	1,339	0.0083	3.48

*Primary test conditions.

Both the static and oscillatory deflections of the
sting were used to correct the data for sting bending
effects. The sting oscillation was essentially in-phase
with the model oscillation, and had an approximate ampli-
tude of ±0.01 in. at the cross flexure pivot. The method
used to reduce the data may be found in Refs. [15], [17],
and [18]. Reference [17] describes the method by which the
sting oscillations were accounted for.

All moments are calculated in the body-axis system,
and are referenced to the cross flexure pivot axis (moment
reference axis).

III.   Uncertainty of Measurements

Propagation of the bias and precision errors of
measured data through the calculated data was made in
accordance with Ref. [19]. Uncertainties in both the
measured and calculated data are given in Table 2.

The quoted uncertainties are based upon steady-
state operation and do not account for the effects of the
support boom vibrations and/or unsteady flow phenomena. No
attempt was made to assess or correct for these effects.
In some instances the pitch-damping derivatives $(C_{m_q} + C_{m_{\dot{\alpha}}})$
exhibited repeatability on the order of 15 to 20 percent,
but in general, the repeatability was about the same as the
quoted uncertainty in Table 2.

Table 2. Uncertainty in the Aerodynamic Parameters

Parameter	Range	Uncertainty
PT, psfa	0 to 1,500 psfa	$\pm$(0.2% + 1.3 psf)
	1,500 to 4,000 psfa	$\pm$4.3 psf
TT, °R	All	$\pm$0.77
PB, psfa	All	$\pm$(0.14% + 3 psf)
α, deg	All	$\pm$0.1
M*	M = 0.6	$\pm$0.005
	M = 0.9	$\pm$0.004
	M = 1.1	$\pm$0.004
	M = 1.3	$\pm$0.004
P, psf*	M = 0.6	$\pm$3.7 psf
	M = 0.9	$\pm$2.7 psf
	M = 1.1	$\pm$2.4 psf
	M = 1.3	$\pm$2.3 psf
Q, psf*	M = 0.6	$\pm$4.7 psf
	M = 0.9	$\pm$3.0 psf
	M = 1.1	$\pm$2.3 psf
	M = 1.3	$\pm$1.8 psf
V, ft/sec*	M = 0.6	$\pm$5.3 ft/sec
	M = 0.9	$\pm$4.1 ft/sec
	M = 1.1	$\pm$3.6 ft/sec
	M = 1.3	$\pm$3.2 ft/sec
Re_D x10^{-6}*	M = 0.6	$\pm$0.014
	M = 0.9	$\pm$0.008
	M = 1.1	$\pm$0.007
	M = 1.3	$\pm$0.006
$C_{m_q} + C_{m_{\dot\alpha}}$*	All	5% (maximum)
C_m	All	4% (maximum)
$\omega D/2V$	All	1.5% (maximum)

*Primary test conditions only.

The static stability derivative (local slope of the pitching moment curve, C_{m_α}) is proportional to the difference of the square of the model aerodynamic frequency and the square of the tare frequency. Since the frequency difference was less than 2 percent for the majority of the data, the estimated uncertainty in the static stability derivative was relatively large. In addition, the sting oscillation corrections used in the reduction of the static stability derivative data were of the same magnitude or larger than the static stability derivative aerodynamic effects. For these reasons, the static stability derivative data are not presented.

CHAPTER V

RESULTS AND ANALYSIS

Since it is well documented in Refs. [1], [2], and [3] that interference effects are dependent upon the state of the boundary layer at the model base, an investigation was conducted at the beginning of the test to determine the type of boundary layer on the model. The method used to determine the model boundary layer and the results of the boundary layer investigation are discussed in the Appendix. Based on the results in the Appendix, it was concluded that the state of the boundary layer over the aft portion of the model was turbulent (boundary layer transition was on the model) for all Reynolds numbers tested at Mach numbers 0.6 and greater.

A limited investigation of increased Reynolds number and frequency effects on interference-producing configurations was also performed. Data obtained at Reynolds numbers that were twice the values of the primary test condition Reynolds numbers did not indicate any influence on critical sting lengths when compared with data obtained at the primary test conditions. Moreover, data obtained at a frequency that was one-half the value of the primary test condition frequency (only Mach numbers 0.2, 0.6, and 0.9 were investigated) also did not reveal any critical sting

length dependency on frequency. However, this conclusion may not be valid at higher frequencies.

At the beginning of the test, it was assumed that interference effects would be greatest at $\alpha = 0$. Since previously obtained data on the present model from Refs. [2] and [3] indicated that interference effects were greatest at $\alpha = 0$ for supersonic and hypersonic Mach numbers, this criterion was also assumed to be true at subsonic and transonic Mach numbers.

In Figs. 15 through 18, the pitch-damping derivatives $(C_{m_q} + C_{m_{\dot\alpha}})$ and base pressure (represented by the base pressure ratio PB/P) are plotted as a function of the effective sting length ratio (L_S/D) for an angle of attack of zero for Mach numbers 0.6, 0.9, 1.1, and 1.3, respectively. The critical sting length ratio (L_{cr}/D) is called out by an arrow on each plot. For all data presented in Figs. 15 through 18, a relatively constant measurement level was found for the sting length ratios greater than or equal to the critical sting length ratio. An abrupt change was noted at a sting length ratio less than the critical value and in the range 1.0 to 3.0. The sting length ratio corresponding to the critical was found to depend upon the Mach number and type of measurement $(C_{m_q} + C_{m_{\dot\alpha}}$ or PB/P). The critical sting length (L_{cr}) determined from the measurement of base pressure is always greater than the value of L_{cr} determined from the measurement of the damping derivatives, being 1.0 model diameters
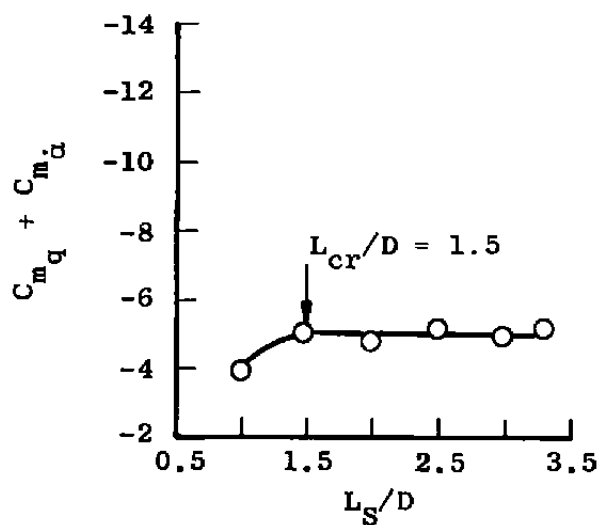
a. Pitch-damping derivatives
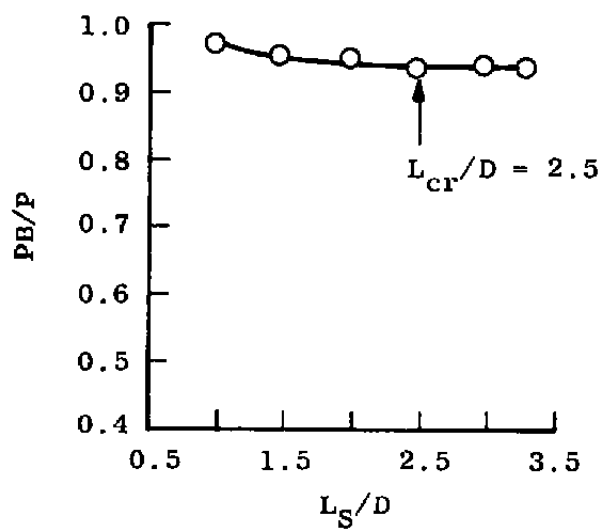
b. Base pressure

Figure 15. Sting length interference effects at
M = 0.6 for α = 0.

43

a. Pitch-damping derivatives
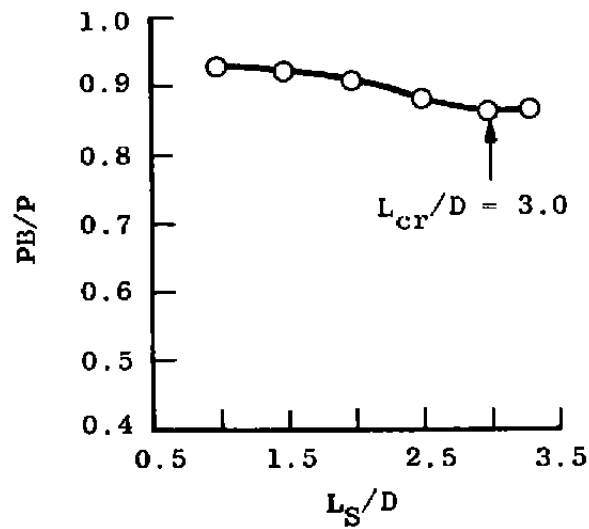
b. Base pressure

Figure 16. Sting length interference effects at
M = 0.9 for α = 0.

44
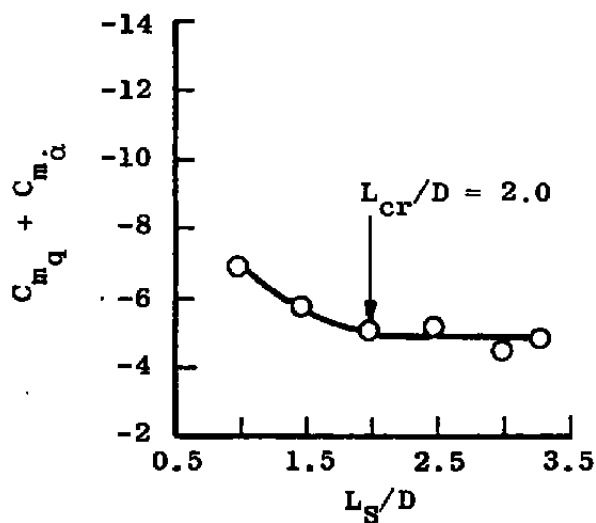
a. Pitch-damping derivatives
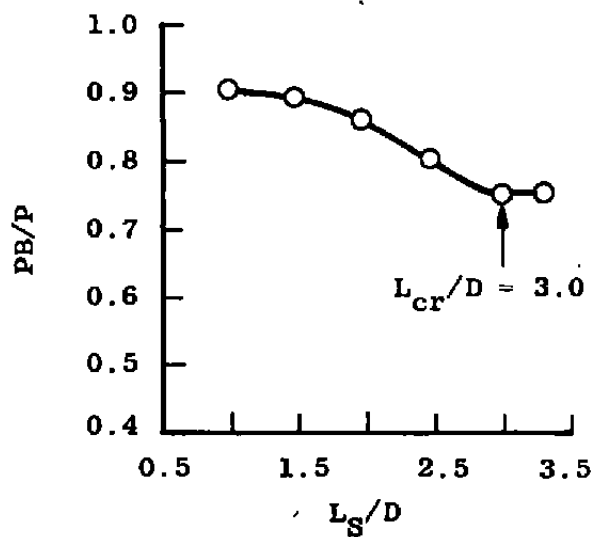
b. Base pressure
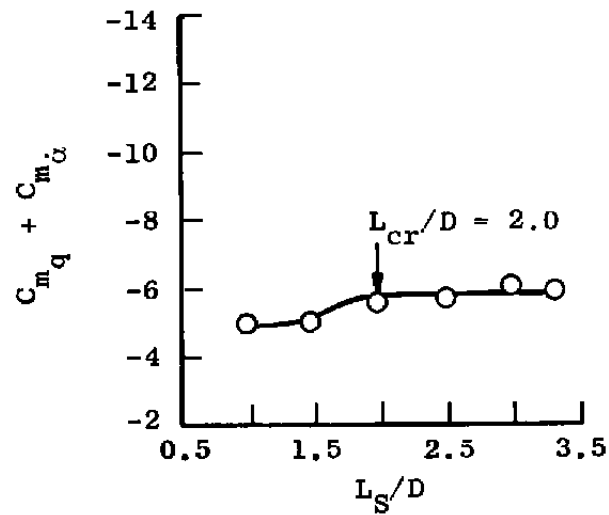
Figure 17. Sting length interference effects at
M = 1.1 for $\alpha = 0$.
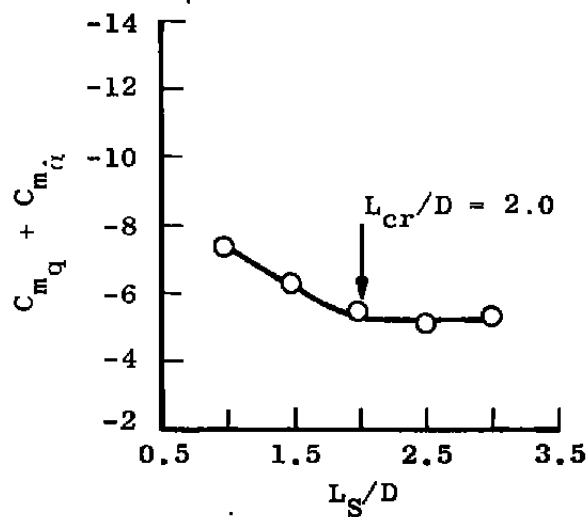
a. Pitch-damping derivatives
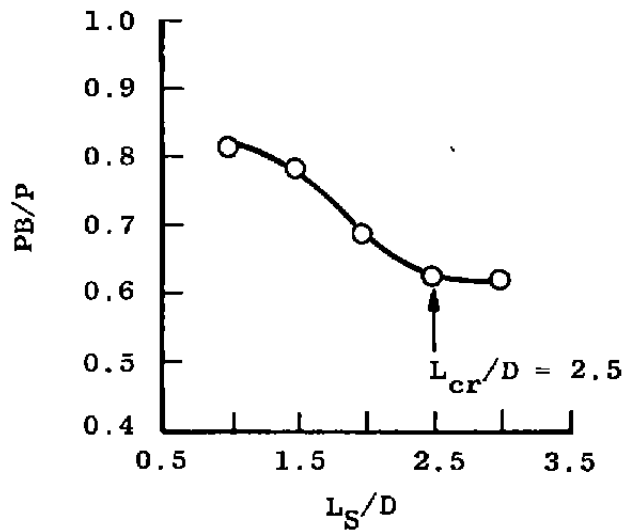
b. Base pressure

Figure 18. Sting length interference effects at
M = 1.3 for α = 0.

46

longer at M = 0.6, 0.9, and 1.1, and 0.5 diameters longer
at M = 1.3. In reviewing Figs. 15 through 18, it is con-
cluded that an L_S/D of 3.0 is sufficient to minimize sting
length interference on both measurements for the Mach
numbers investigated.

Decreasing the sting length from three to one model
diameter for Mach numbers less than 1.0 (Figs. 15 and 16)
resulted in decreased dynamic stability, whereas at Mach
numbers greater than 1.0 (Figs. 17 and 18), the dynamic
stability increased due to interference. Base pressure was
found to increase at all Mach numbers.

To better understand the interference damping
trends, Fig. 19 was prepared. In Fig. 19, the turning
angle of the flow over the shoulder of the model and the
associated flow reattachment point on the flare are sketched
for the various sting lengths tested at M = 1.3. These
sketches are based on the measured tunnel free-stream con-
ditions (as presented in Table 1, page 37) and the measured
base pressure. The Mach number along the shoulder of the
cone (M_1), surface pressure (PS), and turning angle of the
Prandtl-Meyer expansion (ν) were obtained from inviscid,
compressible flow theory [20]. Comparing Fig. 18 with
Fig. 19, the dynamic stability is shown to remain rela-
tively constant at an L_S/D of 3.0, 2.5, and 2.0
(corresponding to Figs. 19a, b, and c, respectively)
because the flow reattachment point is located on the

Measured PB, psi	L_S/D	PB/PT	M_2	ν, deg
2.0	3.0	0.223	1.63	11.44
2.0	2.5	0.223	1.63	11.44
2.22	2.0	0.247	1.57	9.66
2.54	1.5	0.283	1.47	6.71
2.64	1.0	0.294	1.45	6.13

Note: Calculated values of M_2 and ν were obtained from Ref. 120|

M = 1.3 →

(Free Stream)

Q = 3.85 psi
P = 3.26 psi
PT = 9.03 psi
PS = 3.56 psi

a. $L_S/D = 3.0$

b. $L_S/D = 2.5$

c. $L_S/D = 2.0$

d. $L_S/D = 1.5$

e. $L_S/D = 1.0$
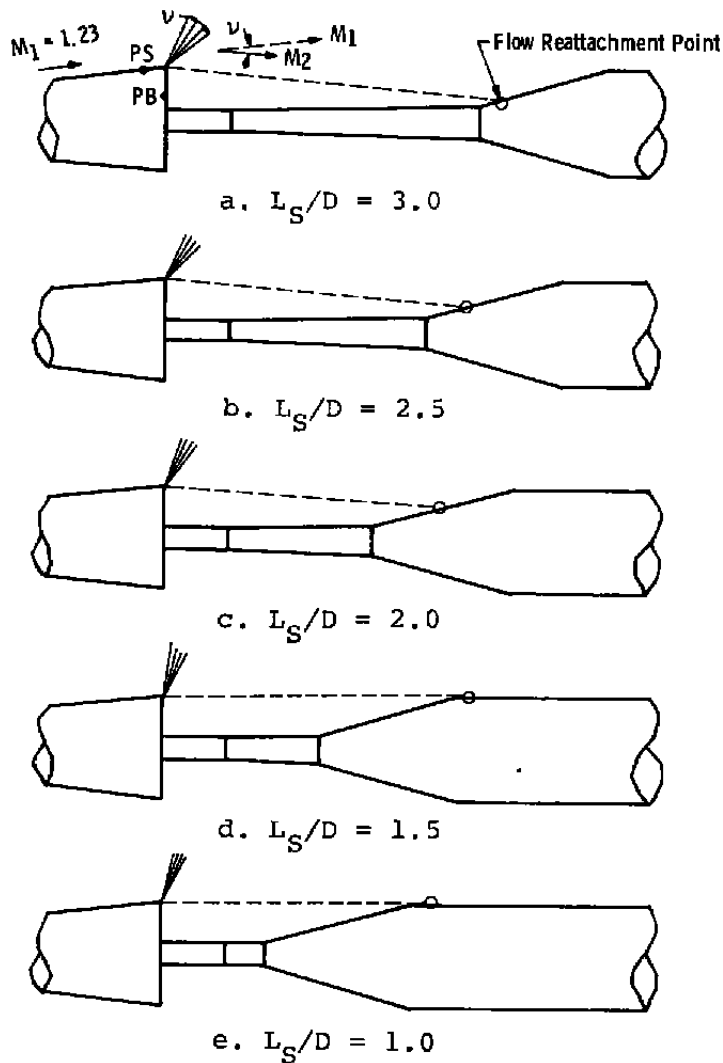
Figure 19. Calculated flow reattachment points on the flare for various sting lengths (M = 1.3).

48

sloped portion of the flare and is free to move as the model oscillates. However, as the L_S/D is decreased to 1.5 or 1.0 (Figs. 19d and e), the reattachment point is effectively fixed beyond the shoulder of the flare. For this case the resultant oscillation causes a slightly decreased turning angle (ν) on the leeside model shoulder. A corresponding increase in ν also occurs on the windward side.

This influence on turning angles at the model shoulder results in an unequal base pressure loading, which in turn results in an increased damping effect. But, the extent to which this unequal base pressure loading influences the overall model damping is not known. It is the author's opinion, however, that this is a dominant effect, based on the static base pressure measurements of Lee and Summers [4] described later in this chapter (page 55).

This analysis is not valid at subsonic Mach numbers because there are no shocks or Prandtl-Meyer expansions on the model, and because the entire model surface pressure distribution can be influenced. However, the wake thickness is much larger than the supersonic case, and vortex shedding is more pronounced. Since the presence of the flare at small values of L_S/D would thicken the wake and thus enhance the vortex-induced based loads, the author believes that these effects are responsible for the observed decrease in dynamic stability at subsonic Mach numbers.

49

Now that the interference effects at $\alpha = 0$ have been discussed, the effects of sting length interference on data obtained at angles of attack up to 20 deg will be presented. Pitch-damping derivatives, static pitching moment (C_m) and base pressure data are presented in Figs. 20 through 23 as a function of angle of attack for various sting length ratios. For all data in these figures, it is shown that, in general, the interference effects on all measurements are smaller at high angles of attack than at low angles of attack. This is as expected, based on the discussion previously presented along with Figs. 7a and d, page 21.

The static pitching moment data generally exhibited sting length dependence over the angle of attack range, except for Mach numbers greater than 0.9, where no dependence on sting length was found. Sting length interference on the measurement of base pressure was generally a maximum at $\alpha = 0$, with interference decreasing as angle of attack was increased. Even at angles of attack greater than zero, the measurement of base pressure was always more sensitive to interference than the other measurements.

The measurement of pitch-damping derivatives in Figs. 20 through 23 also shows that this angle of attack effect is influenced by Mach number. The damping data at M = 1.3 (Fig. 23a) show that at angles of attack of 16 deg and greater, the level of damping obtained for an L_s/D of

Sym	L_S/D
□	1.0
▽	1.5
△	2.0
◁	2.5
◇	3.0
○	3.3
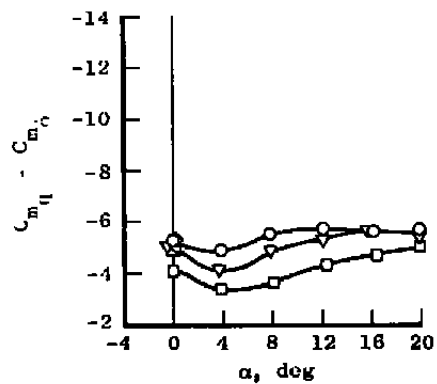
a. Pitch-damping
   derivatives
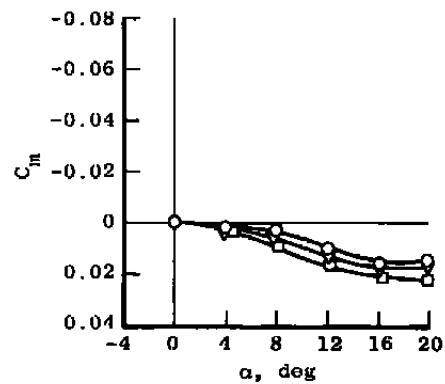
b. Pitching moment
   coefficient
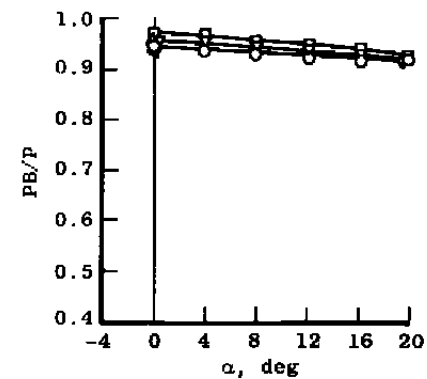
c. Base pressure

Figure 20.   Sting length interference effects as a function of
            angle of attack at M = 0.6.

Sym	L_S/D
□	1.0
▽	1.5
△	2.0
◁	2.5
◇	3.0
○	3.3

a. Pitch-damping
    derivatives

b. Pitching moment
    coefficient
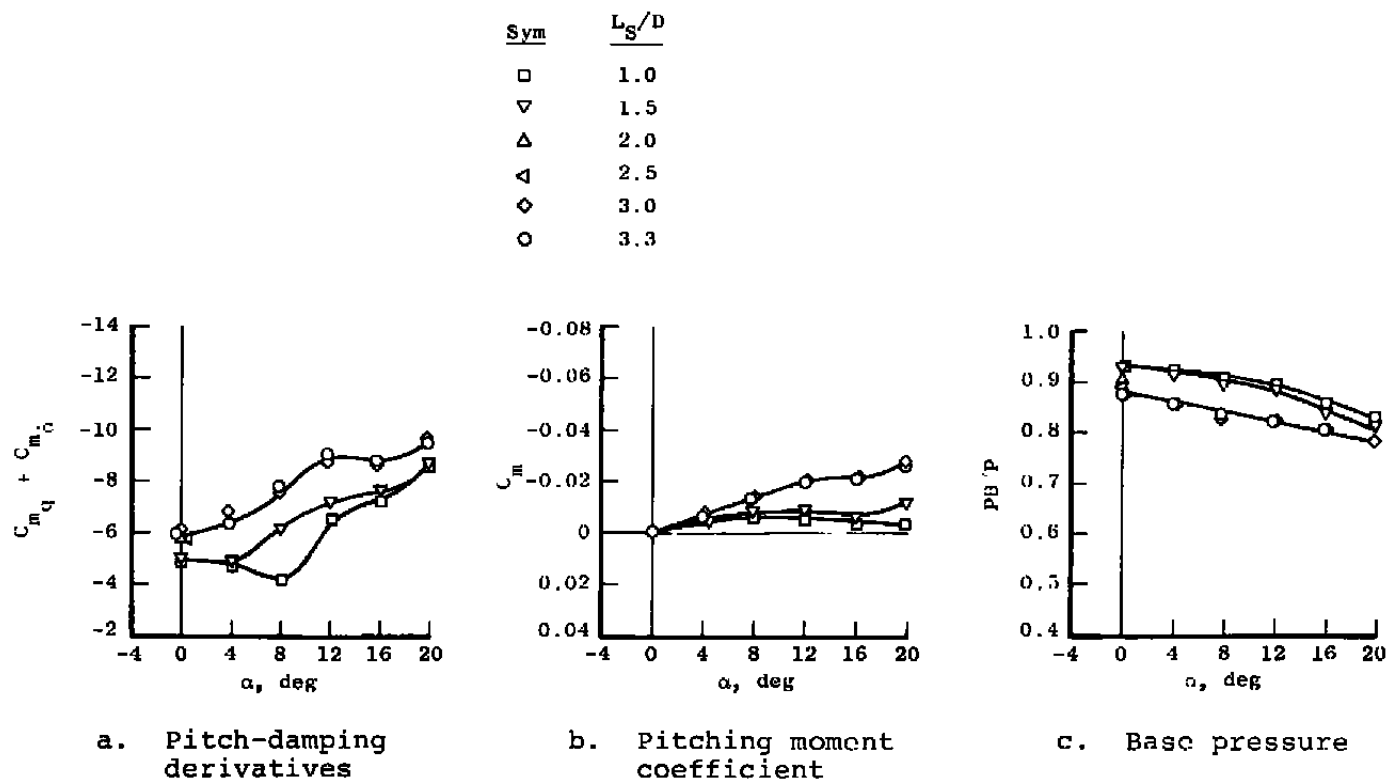
c. Base pressure

Figure 21.   Sting length interference effects as a function of
             angle of attack at M = 0.9.

Sym	L_S/D
□	1.0
▽	1.5
△	2.0
◁	2.5
◇	3.0
○	3.3
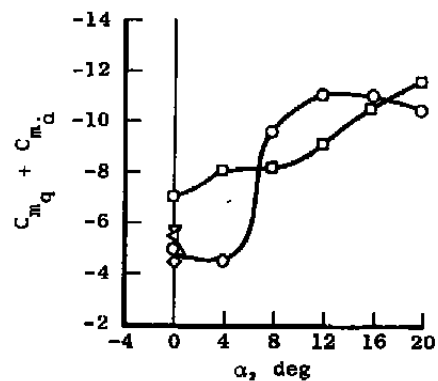
a. Pitch-damping
    derivatives
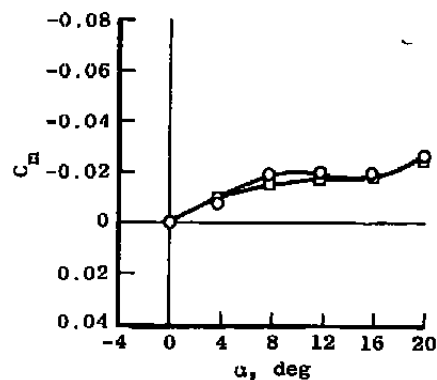
b. Pitching moment
    coefficient
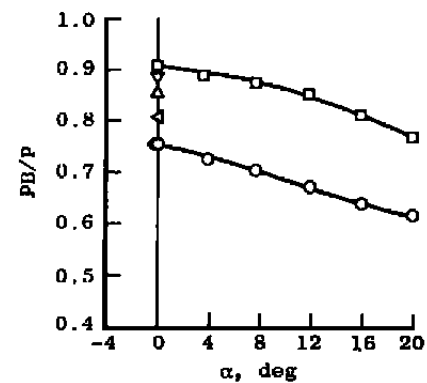
c. Base pressure

Figure 22.   Sting length interference effects as a function of
             angle of attack at M = 1.1.

Sym	L_S/D
□	1.0
▽	1.5
△	2.0
◁	2.5
◇	3.0
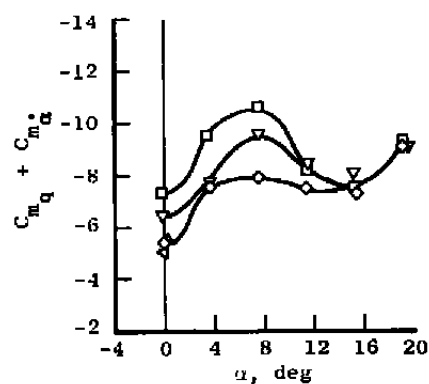
a. Pitch-damping
   derivatives
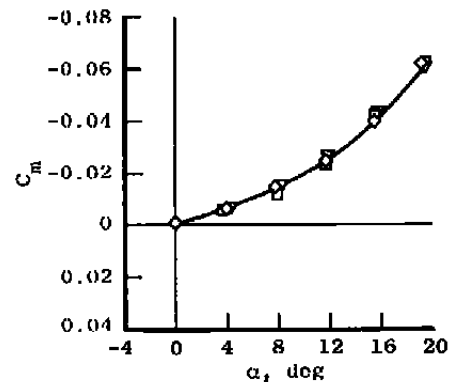
b. Pitching moment
   coefficient
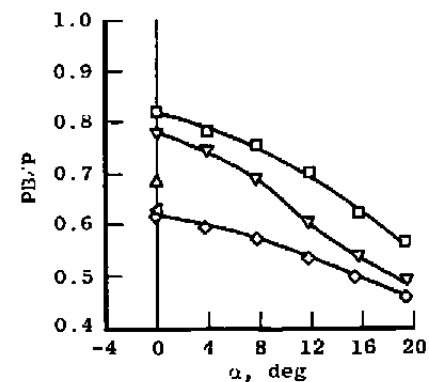
c. Base pressure

Figure 23. Sting length interference effects as a function of
angle of attack at M = 1.3.

1.0 is the same as that obtained for an L_S/D of 3.0; whereas, at M = 0.6 (Fig. 20a), an L_S/D of 1.0 shows some interference at an angle of attack of 20 deg. This trend is reasonable because downstream disturbances would not be expected to propagate as far upstream at supersonic speeds as they would at subsonic speed.

Although interference effects generally decrease as angle of attack increases, Figs. 20a and 21a indicate that the pitch-damping derivatives may in some instances have a slightly greater interference effect in the angle of attack range $0 < \alpha \leq 12$ deg than at $\alpha = 0$ for Mach numbers less than 1.10. This is likely caused by the asymmetric formation of the wake due to the relative proximity of the flare. Small angles of attack would then enhance the unequal loads on the edge of the model base caused by the flare.

It is evident from Figs. 20b and 21b that sting interference effects are statically de-stabilizing as angle of attack is increased for Mach numbers less than 1.1. However, at Mach numbers 1.1 and 1.3 (Figs. 22b and 23b), interference has practically no effects on static stability. These findings may be explained better when compared with surface pressure coefficient (C_p) data obtained by Lee and Summers [4] on a cylindrical model. At Mach numbers 0.6 and 1.0, Lee and Summers found that as L_S/D was decreased from 9.8 to 0, the C_p on the shoulder of the model near the base increased significantly. Moreover, at M = 1.4, they

55

found essentially no change in C_p. Thus, the change in static stability shown in Figs. 20b and 21b is due to an increased pressure distribution on the aft end of the model shoulder. At increased angles of attack, the leeside pressure distribution is greater than the pressure distribution on the windward side, resulting in the observed statically de-stabilizing effect. Consequently, no interference effects on static stability are observed at $\alpha = 0$ because the increased pressure distributions on both the leeward and windward side are equal.

The same trend of dynamic interference with Mach number that was found at $\alpha = 0$ (page 47) was also observed at angles of attack up to 20 deg, with one exception: Mach number 1.1 at angles of attack from 8 to 16 deg (Fig. 22a). Because of the limited amount of data, a confident explanation of this exception is not known. However, it is believed that the complex flow field in the base region at Mach number 1.1 is subject to abrupt changes at increased angles of attack, and that these abrupt changes would be reflected in the damping measurements.

At all Mach numbers, interference caused by the flare increased the base pressure ratio (Figs. 20c, 21c, 22c, and 23c). This increase in base pressure is expected at small values of L_S/D because of the increased thickness of the wake neck (recompression region) due to the flare.

In analyzing the data in Figs. 15 through 18, pages 43 through 46, and Figs. 20 through 23, pages 51 through 54,

it is evident that an investigation of sting length inter-
ference effects only at $\alpha = 0$ can be considered fairly
accurate for predicting the maximum sting length inter-
ference effects over the angle of attack range $0 \leq \alpha < 20$ deg.
Thus, defining critical sting length based only on data at
$\alpha = 0$ can still be considered useful for indicating sting
length interference effects in general.

CHAPTER VI

COMPARISON OF RESULTS

Based on the data presented in Figs. 15 through 18,
pages 43 through 46, and Figs. 20 through 23, pages 51
through 54, the appropriate values of the critical sting
length ratio were determined, and the results are plotted
in Fig. 24 as a function of Mach number. Also shown in
Fig. 24 are the results of Refs. [2] and [3], to depict the
variation of critical sting length over the subsonic to
hypersonic range for a turbulent boundary layer. The
shaded area called out on the plot of L_{cr}/D, as determined
by the measurement of pitching moment (Fig. 24b), is due to
an insufficient amount of data. In analyzing the data in
Figs. 20b, 21b, and 22b, the critical sting length ratio,
as determined by the measurement of pitching moment, is
certainly in the shaded area. However, the dashed line in
the shaded area indicates the most probable values of
L_{cr}/D.

A review of Fig. 24 shows that a critical sting
length of two model diameters is suitable over the Mach
number range 0.6 to 3.0 for the measurement of damping
derivatives. The critical sting length determined by the
measurement of the static pitching moment varies from two
model diameters at Mach number 0.6, to one model diameter
at Mach numbers greater than 1.1. The measurement of base

58

Sym | Data Source | 7-deg Cone, 15-percent Bluntness
O | Present Investigation | $\theta = \pm 1$ deg, $D_S/D = 0.22$, $\theta_S = 15$ deg
● | Refs. [2] and [3]

Turbulent Boundary Layer

$0 < \alpha \le 12$ deg

$\alpha = 0$ Unless Otherwise Noted

Considering Data at $\alpha = 0$ Only

a. Measurement of $C_{m_q} + C_{m_{\dot{\alpha}}}$

Uncertainty Region Due to Insufficient Data

Estimated

$\alpha = 0$ to 16 deg ← | → $\alpha = 0$ to 8 deg

b. Measurement of C_m

$\alpha = 0$

c. Measurement of PB/P
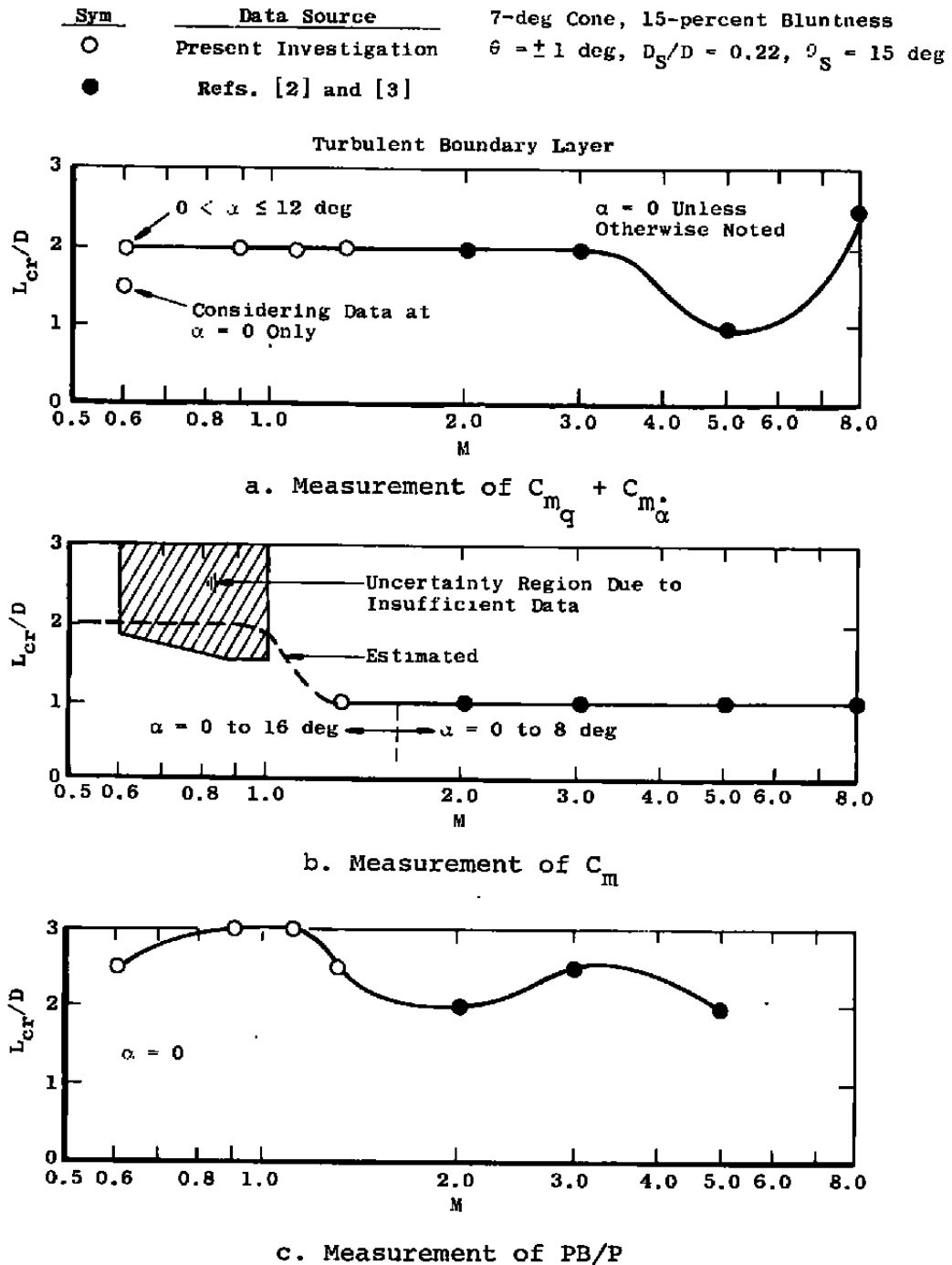
Figure 24.   Variation of critical sting length with Mach number for various measurements.

pressure indicates that a critical sting length of two to three model diameters is required.

Based on the data in Fig. 24, a critical sting length of three model diameters is satisfactory regardless of the type of measurement. Base pressure seems to indicate the longest critical sting length, which is generally 25 to 50 percent higher than the critical sting length determined by static pitching moment or pitch-damping derivatives. Thus, the static pitching moment and pitch-damping derivatives should be free from sting length interference effects for sting lenghts greater than or equal to the critical sting length determined by base pressure measurements.

Critical sting length data from other reference sources were sought to compare with the critical sting length data determined from the present investigation. Only one critical sting length evaluation on damping derivative measurements at subsonic-transonic speed for a blunt, flat-base cone was found. This was reported by Wehrend [21], who found no sting length effects for a blunt, flat-base cone (e.g., $L_{cr}/D = 0$) at Mach numbers 0.65 and 1.0 for the sting lengths he investigated. Wehrend also found no interference effects due to sting diameter. Both Uselton [2] and Ericsson [10] discussed the applicability of Wehrend's results. Uselton stated that Wehrend's data should be used with caution because the interference hardware used may have affected the measurements. Ericsson

suggested that Wehrend's interference results were not representative of turbulent flow over the model base and that Wehrend's data were influenced by transition-amplified interference effects. As compared to the large amount of data obtained during the present investigation, it is also possible that Wehrend's conclusions were based on a rather limited quantity of data.

A substantial amount of critical sting length data for base pressure measurements for similar tests was found. Figure 25 presents critical sting length data from various sources [4, 5, 9], including the present data, for Mach numbers 0.6 to 2.4. It is evident in Fig. 25 that the critical sting length for the measurement of base pressure is highly dependent on the sting diameter ratio (D_S/D) and flare angle (θ_S) in the subsonic and transonic range. At supersonic Mach numbers ($M \geq 1.6$), the parameters D_S/D and θ_S do not appear to affect critical sting length significantly. In Fig. 25a, the critical sting length data for $\theta_S = 15$ deg in the subsonic region (present data) are lower than all other data. This is probably because of the relatively small D_S/D (0.22) for the present test as compared to the data from the other sources ($D_S/D = 0.5$). Although only one D_S/D was used for the present test, it appears that this D_S/D (0.22) did provide a negligible or minimal (within the measurement uncertainty) interference effect. This comparison gives some credibility to the

61

Sym	θ_S, deg	D_S/D	Data Source	Model
◊	2.5	0.33	Ref. 5	5-caliber Cone-Cylinder
—·—·—	4	0.50	Ref. 4	10-caliber Ogive-Cylinder
□	5	0.33	Ref. 5	5-caliber Cone-Cylinder
———	8	0.50	Ref. 4	10-caliber Ogive-Cylinder
△	10	0.33	Ref. 5	5-caliber Cone-Cylinder
	12	0.50	Ref. 4	10-caliber Ogive-Cylinder
○	15	0.22	Present and Ref. 3	7-deg Cone, 15-percent Bluntness
◁	15	0.33	Ref. 5	5-caliber Cone-Cylinder
◁	15	0.50	Ref. 9	9.15-caliber Ogive-Cylinder
◇	20	0.33	Ref. 5	5-caliber Cone-Cylinder

Note: All ogive- or cone-cylinder models had no boattail.
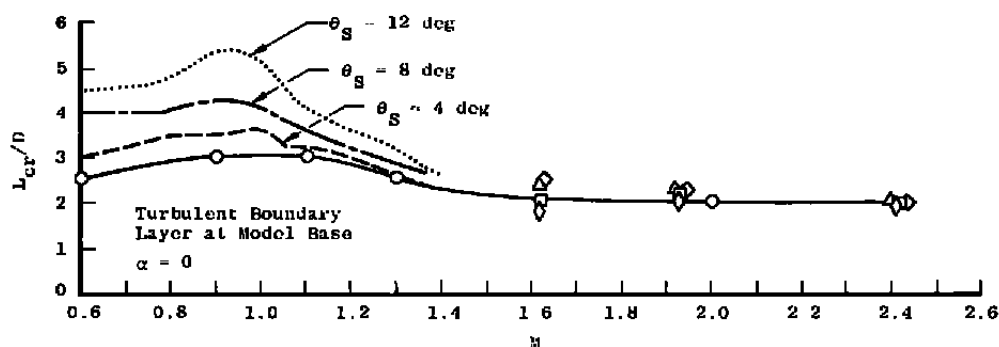
a. Effect of flare angle
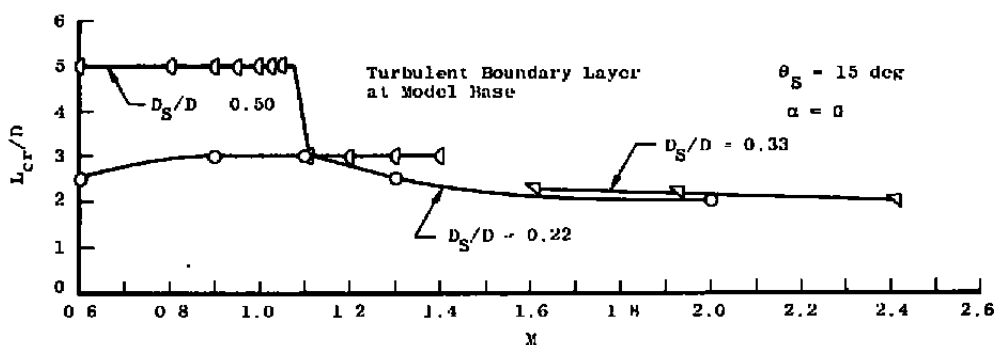
b. Effect of sting diameter

Figure 25. Comparison of critical sting length defined by base pressure measurements.

62

two-dimensional analogy discussed on page 16, which indi-
cated that sting diameter effects are primarily a subsonic
phenomenon. However, the data in Fig. 25a also tends to
indicate that the effects of θ_S are more pronounced at
subsonic and transonic Mach numbers.

CHAPTER VII

CONCLUDING REMARKS

An investigation was conducted to determine sting length interference effects on the measurement of dynamic stability derivatives and base pressure on a conical model in transonic flow. The boundary layer at the model base was turbulent. The Mach number was varied from 0.6 to 1.3, at a Reynolds number, based on model diameter, of approximately 1.7 million. Angles of attack from 0 to 20 deg were tested. The model was a flat, open base, 7-deg cone with a nose bluntness ratio of 15 percent.

Data from this investigation were compared with data obtained from various sources, and a discussion of the causes of interference was presented. Based on the results of this investigation, the following conclusions were made:

1. Critical sting length, as determined by the measurement of pitch-damping derivatives and static pitching moment at subsonic to transonic speeds, is less than or equal to two model diameters.

2. Critical sting length, as determined by the measurement of base pressure (used in the calculation of base drag), is generally three model diameters for Mach numbers 0.6 to 1.3, and generally was found to be 25 to 50 percent

greater than the critical sting length
determined by the measurements of static or
dynamic moments.

3. In general, critical sting length is a maximum
    at $\alpha = 0$, and decreases as angle of attack
    increases.

From an analysis of the results of this investi-
gation, a discussion of the causes of interference, and a
comparison of other sources of data, the following guide-
lines for predicting sting interference are proposed:

1. At subsonic and transonic Mach numbers, the
    measurement of base pressure can be a practical
    indicator of sting interference effects on
    static and dynamic moment measurements, although
    it tends to be slightly conservative.

2. Below the neighborhood of Mach number 1.5, the
    critical sting length appears to be a strong
    function of both the sting diameter and the
    flare angle. It appears that critical sting
    length increases as both sting diameter and
    flare angle increase. Above Mach number 1.5,
    the critical sting length appears to be
    relatively independent of either sting diameter
    or flare angle.

3. The data in Fig. 24, page 59, and Fig. 25,
    page 62, should be used as a guide for indi-
    cating the relative interference effects on
    various measurements for similar models tested
    in similar test conditions.

BIBLIOGRAPHY

1. Whitfield, Jack D. "Critical Discussion of Experiments on Support Interference at Supersonic Speeds," Arnold Engineering Development Center TN-58-30, Arnold Air Force Station, Tennessee, August, 1958.

2. Uselton, Bob L., and Fred B. Cyran. "Critical Sting Length as Determined by the Measurement of Pitch-Damping Derivatives for Laminar, Transitional, and Turbulent Boundary Layers at Mach Number 3 for Reduced Frequencies of 0.0033 and 0.0056," Arnold Engineering Development Center TR-77-66, Arnold Air Force Station, Tennessee, July, 1977.

3. Uselton, Bob L., and Fred B. Cyran. "Sting Interference Effects as Determined by Measurements of Dynamic Stability Derivatives, Surface Pressure, and Base Pressure for Mach Number 2 through 8," Arnold Engineering Development Center TR-79-89, Arnold Air Force Station, Tennessee, December, 1979.

4. Lee, George, and James L. Summers, "Effects of Sting-Support Interference on the Drag of an Ogive-Cylinder Body with and without a Boattail at 0.6 to 1.4 Mach Numbers," National Advisory Committee for Aeronautics RM-A57I09, Ames Aeronautical Laboratory, Moffett Field, California, December, 1957.

5. Love, Eugene S. "A Summary of Information on Support Interference at Transonic and Supersonic Speeds," National Advisory Committee for Aeronautics RM-L53K12, Langley Aeronautical Laboratory, Langley, Virginia, January, 1954.

6. Reese, David E., Jr., and William R. Wehrend, Jr. "Effects of Sting-Support Interference on the Base Pressures of a Model Having a Blunt-Nosed Cylinder Body and a Conical Flare at Mach Numbers of 0.65 to 2.20," National Aeronautics and Space Administration TM X-161, Ames Research Center, Moffett Field, California, February, 1960.

7. Jaffe, Peter. "A Free-Flight Investigation of Transonic Sting Interference," National Aeronautics and Space Administration TM 33-704, Jet Propulsion Laboratory, California Institute of Technology, Pasadena, California, January, 1975.

8. Tunnell, Phillips J. "An Investigation of Sting Support Interference on Base Pressure and Forebody Chord Force at Mach Numbers from 0.60 to 1.30," National Advisory Committee for Aeronautics RM-A54K16a, Ames Aeronautical Laboratory, Moffett Field, California, January, 1955.

9. German, R. C. "Strut Support Interference on a Cylindrical Model with Boattail at Mach Numbers from 0.6 to 1.4," Arnold Engineering Development Center TR-76-40, Arnold Air Force Station, Tennessee, May, 1976.

10. Ericsson, Lars E. "Modification of Aerodynamic Prediction of the Longitudinal Dynamics of Tactical Weapons, Lockheed Missile and Space Company, Inc., D646354, Sunnyvale, California, June, 1979.

11. Chapman, Dean R. "An Analysis of Base Pressure at Supersonic Velocities and Comparison with Experiment," National Advisory Committee for Aeronautics TN-2137, Ames Aeronautical Laboratory, Moffett Field, California, July, 1950.

12. Nash, J. F., V. G. Quincey, and J. Callinan. "Experiments on Two-Dimensional Base Flow at Subsonic and Transonic Speeds," Ministry of Aviation Aeronautical Research Council Reports and Memoranda No. 3427, printed and published by Her Majesty's Stationery Office, London, England, January, 1963.

13. Reding, J. Peter, and Lars E. Ericsson. "Dynamic Support Interference," Journal of Spacecraft and Rockets, 10(No. 7):547-553, July, 1972.

14. Test Facilities Handbook. Eleventh edition. Vol. 4. Arnold Air Force Station, Tennessee: Arnold Engineering Development Center, 1979.

15. Burt, G. E. "A Description of a Pitch/Yaw Dynamic Stability, Forced Oscillation Test Mechanism for Testing Lifting Configurations," Arnold Engineering Development Center TR-73-60, Arnold Air Force Station, Tennessee, June, 1973.

16. Cyran, Fred B. "Sting Interference Effects on a 7-deg Cone as Determined by Measurements of Dynamic Stability Derivatives and Base Pressure for Mach Numbers 0.3 through 1.3," Arnold Engineering Development Center TSR-79-P75, Arnold Air Force Station, Tennessee, December, 1979.

17. Burt, Glen E., and James C. Uselton. "Effects of Sting Oscillations on the Measurement of Dynamic Stability Derivatives," Journal of Aircraft, 13(No. 3):210-216, March, 1976.

18. Schueler, C. J., L. K. Ward, and A. E. Hodapp, Jr. "Techniques for Measurements of Dynamic-Stability Derivatives in Ground Test Facilities," Advisory Group for Aerospace Research & Development AGARDograph 121, North Atlantic Treaty Organization, Paris, France, October, 1967.

19. Thompson, J. W., and R. B. Abernethy, et al. "Handbook Uncertainty in Gas Turbine Measurements," Arnold Engineering Development Center TR-73-5, Arnold Air Force Station, Tennessee, February, 1973.

20. Ames Research Staff. "Equations, Tables, and Charts for Compressible Flow," National Advisory Committee for Aeronautics Report 1135, Ames Aeronautical Laboratory, Moffett Field, California, 1953.

21. Wehrend, William R., Jr. "An Experimental Evaluation of Aerodynamic Damping Moments of Cones with Different Centers of Rotation," National Aeronautics and Space Administration TN D-1768, Ames Research Center, Moffett Field, California, March, 1963.

22. Uselton, B. L. "Investigation of Sting Support Interference Effects on the Dynamic and Static Stability Characteristics of a 10-Deg Cone at Mach Numbers 2.5, 3.0, and 4.0," Arnold Engineering Development Center TDR-64-226, Arnold Air Force Station, Tennessee, November, 1964.

23. Ward, L. K. "Influence of Boundary-Layer Transition on Dynamic Stability at Hypersonic Speeds." Paper No. 9 presented at the Transactions of the Second Technical Workshop on Dynamic Stability Testing, Arnold Engineering Development Center, Arnold Air Force Station, Tennessee, 1965.

24. Uselton, Bob L., and Tom O. Shadow. "Dynamic Stability Characteristics of 3- and 5-cal Army-Navy Spinner Projectiles at Mach Number 0.2 through 1.3," Arnold Engineering Development Center TR-70-115, Arnold Air Force Station, Tennessee, July, 1970.

25. Cyran, Fred B., Bob L. Uselton, and Ed J. Marquart. "Evaluation of Critical Sting Length on a 7-deg Cone as Determined by Measurements of Dynamic Stability Derivatives and Base Pressure for Mach Numbers 0.2 through 1.3," Arnold Engineering Development Center TR-80-17, Arnold Air Force Station, Tennessee, May, 1980.
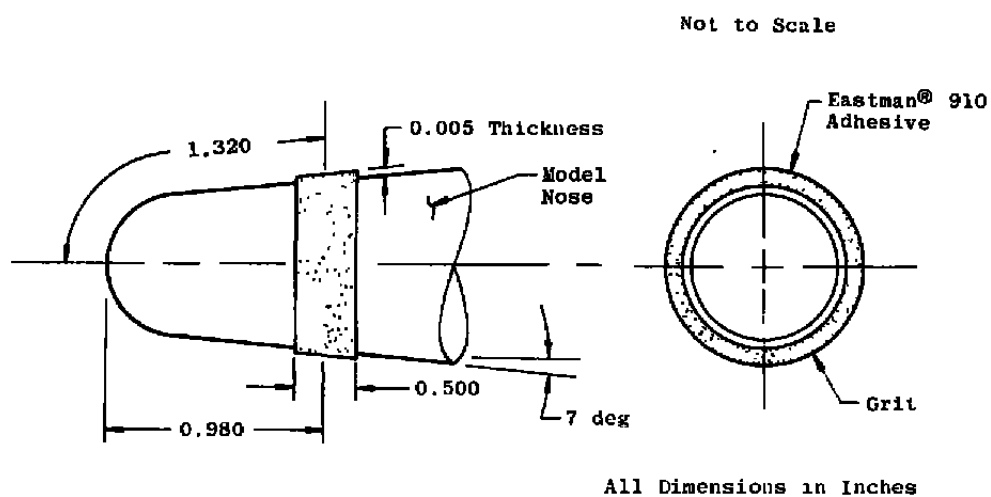
APPENDIX

BOUNDARY LAYER INVESTIGATION

At the beginning of the test, data were obtained
at various Reynolds numbers and with two different
boundary layer trips (Fig. A-1) at selected Mach numbers
to determine their effects on the measured aerodynamic
results. The determination of the state of the model
boundary layer was made by comparing pitch-damping
derivatives and base pressure with and without trips at
the different Reynolds numbers.

For supersonic and hypersonic Mach numbers, the
effects of the state of the model boundary layer on pitch-
damping derivatives and base pressure are well known.
Typical variations of these two measurements with Reynolds
number, obtained from Ref. [3] for the present model at
Mach number 5.0, are shown in Fig. A-2. The dashed line
shows the expected trends, based on similar models for
supersonic and hypersonic Mach numbers, that are reported
in Refs. [22] and [23]. An increase in damping was found
when transition occurred near the model base. As the
Reynolds number was increased, transition moved forward
on the model, resulting in turbulent flow on the shoulder
of the model. This caused the damping to decrease to about
the same level as the laminar flow data. The presence of a
boundary layer trip provided turbulent flow at lower .

Not to Scale

1.320

0.005 Thickness

Model Nose

0.500

7 deg

0.980

Eastman® 910 Adhesive

Grit

All Dimensions in Inches

Trip	Grit Size	Average Height of Grit, in.
1	#60	0.012
2	#36	0.020

Figure A-1. Boundary layer trip details.

M = 5 $L_S/D = 3.3$ 15-percent Spherically Blunt,
ωD/2V = 0.0027 $D_S/D = 0.22$ 7-deg Cone with a Flat,
α = 0   Open Base

Open Symbols - No Trips
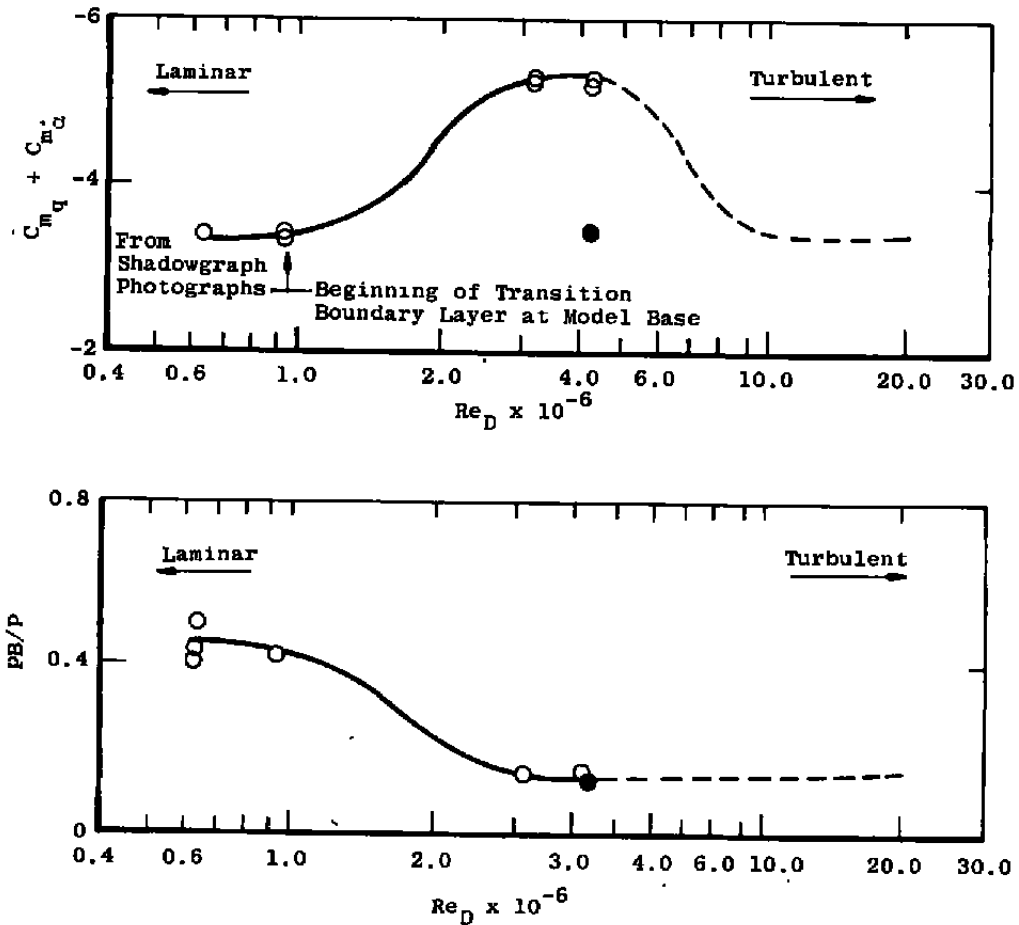Solid Symbols - Tripped

Figure A-2.   Typical trends of damping derivatives and base
              pressure as a function of Reynolds number and
              type of boundary layer [3].

73

Reynolds numbers. The base pressure showed a gradual

decrease as transition moved upstream on the model and

leveled off as fully turbulent flow was established.

In making a comparison between boundary layer

transition effects at subsonic-transonic Mach numbers and

supersonic-hypersonic Mach numbers,it was assumed that some

effect (although not necessarily similar) would occur in

the damping and pressure measurements for a wide Reynolds

number range or when trips were used. The results of a

Reynolds number variation and the effects of boundary layer

trips are shown in Fig. A-3 for Mach numbers 0.2, 0.95,

and 1.3. This investigation of the model boundary layer

was conducted with the clean (no interference-producing

hardware attached) sting configuration and at zero angle of

attack. At Mach number 0.95 and 1.3, both the pitch-

damping derivatives and base pressure ratio were essentially

invariant with Reynolds number. The addition of the

boundary layer trips had virtually no effect on either

measurement. Some effects of Reynolds number on the

damping data were found at Mach number 0.2 at the lower

Reynolds numbers. A similar effect at Mach number 0.2 was

reported in Ref. [24] for a three-caliber Secant-Ogive

cylinder. The base pressure obtained at $M = 0.2$ were not

useful for indicating transition because the base pressure

Sym	Trip	M	$\dfrac{\omega D}{2V}$
◑	None	0.2	0.048
◐	2	0.2	0.048
◑	None	0.95	0.011
▲	1	0.95	0 011
◐	2	0.95	0.011
○	None	1.3	0.008
△	1	1.3	0.008
□	2	1.3	0.008

$\alpha = 0$

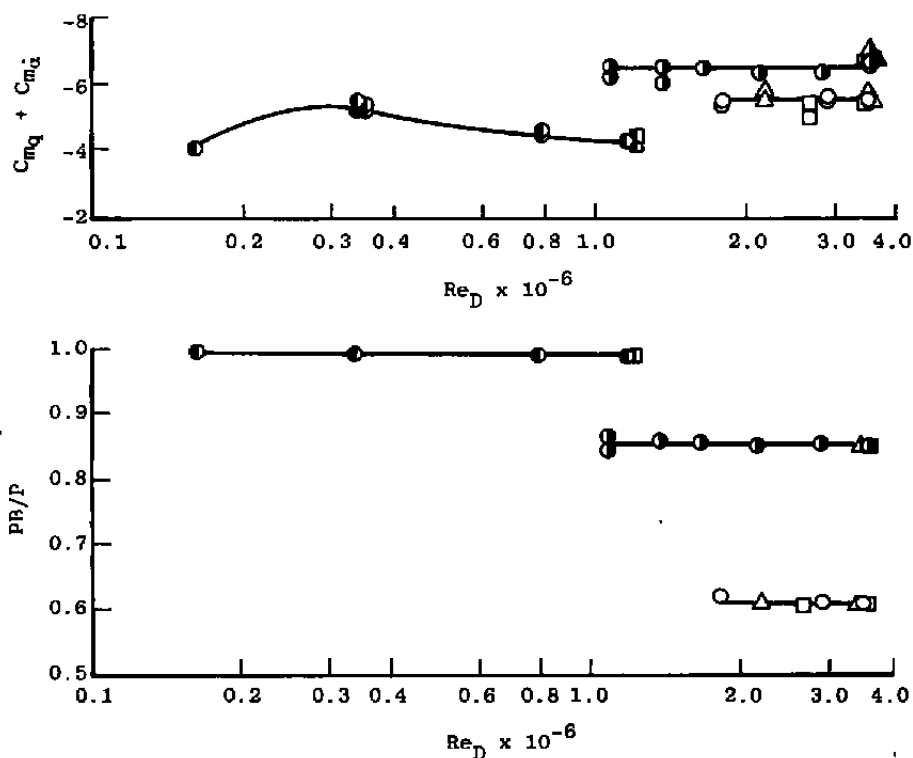$\theta = \pm 1$ deg

$L_S/D \geq 3.0$

Figure A-3. Variation of pitch-damping derivatives and base pressure as a function of Reynolds number at subsonic and transonic Mach numbers.

ratio was very close to unity. It was concluded from Fig. A-3 that the boundary layer ahead of the model base was turbulent for all Reynolds numbers (Re_D) greater than 1.0×10^6.

NOMENCLATURE

A   Reference area (based on model base diameter (D)), 0.349 ft^2

C_{D_B} Base drag coefficient, $-(PB-P)/Q$

C_m Pitching-moment coefficient, pitching moment/$Q \cdot A \cdot D$

C_{m_q} Pitching-moment coefficient due to pitch velocity, $\partial C_m / \partial (qD/2V)$, radian^{-1}

C_{m_α} Pitching-moment coefficient due to angle of attack (slope of the pitching-moment curve), $\partial C_m / \partial \alpha$, radian^{-1}

$C_{m_{\dot{\alpha}}}$ Pitching-moment coefficient due to rate of change of angle of attack, $\partial (C_m) / \partial (\dot{\alpha}D/2V)$, radian^{-1}

C_P Surface pressure coefficient, $(PS-P)/Q$

C_{P_B} Base pressure coefficient, $(PB-P)/Q$

D   Reference length (model base diameter), 0.667 ft

D_f Sting flare diameter (see Fig. 2), in.

D_S Sting diameter at model base, in.

ℓ Trailing plate length (see Fig. 6), in.

L_{cr} Critical sting length, in. (for $L_S < L_{cr}$, model data are affected)

L_S Effective sting length (from model base to sting flare) (see Fig. 11), in.

L_w Distance between the model base and the wake neck (see Fig. 1), in.

M   Free-stream Mach number

M_S Mach number in the external stream after an
           isentropic expansion from P to PB

M_1 Mach number at the shoulder of the cone

M_2 Mach number of the flow following an isentropic
           Prandtl-Meyer expansion

OC   Oscillatory component

P   Free-stream static pressure, psf or psi

PB   Model base pressure, psf or psi

PS   Surface pressure, psf or psi

PT   Tunnel stilling chamber pressure, psfa or psia

q   Pitching velocity, radian/sec

Q   Free-stream dynamic pressure, psf or psi

Re_D Free-stream Reynolds number based on reference
           length (D)

SC   Static component

TT   Tunnel stilling chamber temperature, °R

V   Free-stream velocity, ft/sec

α Angle of attack, deg or radian

$\dot{\alpha}$ Time rate of change of angle of attack, radian/sec

δ Boundary layer thickness, in.

θ Oscillation amplitude, deg

θ_S Sting flare angle (see Fig. 2), deg

ω Oscillation frequency, radian/sec

ν Turning angle of the flow through a Prandtl-Meyer

expansion, deg

$\frac{\omega D}{2V}$ Reduced frequency parameter, radian

$\mathcal{C}_L$ Centerline